Synthesis and Characterization of Mixed Spinel Ferrite Nanoparticles for EMI Applications

By

Anoom Zafar

School of Chemical and Materials Engineering

National University of Sciences and Technology

2023

Synthesis and Characterization of Mixed Spinel Ferrite Nanoparticles for EMI Applications

Name: Anoom Zafar

Registration No: Fall 2020-NSE 8, 0000327010

This thesis is submitted as a partial fulfillment of the requirements for the degree of

Master of Science in Nanoscience and Engineering

Supervisor Name: Dr. Muhammad Siyar

School of Chemical and Materials Engineering (SCME)

National University of Sciences and Technology (NUST)

H-12 Islamabad, Pakistan

March ,2023

THESIS ACCEPTANCE CERTIFICATE

Certified that final copy of MS thesis written by Mr **Anoom Zafar** (Registration No 00000327010), of School of Chemical & Materials Engineering (SCME) has been vetted by undersigned, found complete in all respects as per NUST Statues/Regulations, is free of plagiarism, errors, and mistakes and is accepted as partial fulfillment for award of MS degree. It is further certified that necessary amendments as pointed out by GEC members of the scholar have also been incorporated in the said thesis.

Signature: _____

Name of Supervisor: **Dr Muhammad Siyar**

Date: 15 − 09 − 2023

Signature (HOD): _____

Date: 15/9/23

Signature (Dean/Principal): _____

Date: 15 · 9 · 2023

National University of Sciences & Technology (NUST)
MASTER'S THESIS WORK
Formulation of Guidance and Examination Committee (GEC)

Name: **Anoom Zafar** NUST Regn No: **327010**

Department: **SCME** Specialization: **Nanoscience and engineering**

Credit Hour Completed: **18** 24 CGPA: **3.58** 3.50

Course Work Completed

S/No	Code	Title	Core/Elective	CH	Grade
1	NSE-813	Essentials of Nanoscience and Engineering	Core	3	B+
2	NSE-845	Nanolithography and Device Fabrication	Elective	3	B+
3	MSE-854	Characterization of Materials	Core	3	A
4	MSE-856	Nano Material and Processing	Core	3	B+
5	MSE-872	Composite Materials	Elective	3	A
6	NSE-812	Environmental Nanotechnology	Elective	3	B
7	RM-898	Research Methodology	Additional	2	Q

Exam Br

15/11/21

Date **03-11-2021** Student's Signature _____

Thesis Committee

1. Name: **Dr. Muhammad Siyar** **(Supervisor)** Signature: _____
   Department: **Material & Surface Engineering**

2. Name: **Dr. Malik Adeel Umer (Co-Supervisor)** Signature: _____
   Department: **Material & Surface Engineering**

3. Name: **Dr. Mohsin Saleem** Signature: _____
   Department: **Material & Surface Engineering**

4. Name: **Dr. Zeeshan Ali** Signature: _____
   Department: **Material & Surface Engineering**

Date: **25-11-21** Signature of Head of Department: _____ 25/11/21

APPROVAL

Date: **26.11.2021** _____
Dean/Principal

Distribution
1x copy to Exam Branch, Main Office NUST
1x copy to PGP Dte, Main Office NUST
1x copy to Exam branch, respective institute

School of Chemical and Materials Engineering (SCME) Sector H-12, Islamabad

* 8. NSE-961 Surface coatings & Thin Films Elective 3.0 B+
  9. ESE-828 Functional Nanomaterials for Elective 3.0 B

National University of Sciences &Technology (NUST)

MASTER'S THESIS WORK

We hereby recommend that the dissertation prepared under our supervision by Regn No & Name: 00000327010 Anoom Zafar
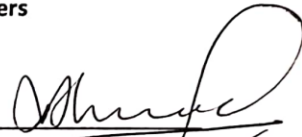
Title: **Synthesis and characterization of mixed spinel ferrite nanoparticles for EMI applications.**

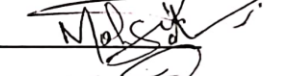Presented on: **07 Sep 2023**   at: **1400 hrs in SCME (Seminar Hall)**

Be accepted in partial fulfillment of the requirements for the award of Masters of Science degree in **Nanoscience & Engineering.**
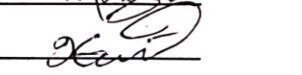
Guidance & Examination Committee Members

Name: **Dr Nasir M Ahmad**   Signature: _____

Name: **Dr Mohsin Saleem**   Signature: _____

Name: **Dr Iftikhar Hussain Gul** (Co-Supervisor)   Signature: _____

Supervisor's Name**: Dr Muhammad Siyar**   Signature: _____

Dated: 07-09-823

Head of Department
Date 14/9/23

Dean/Principal
Date 14·9·2023

School of Chemical &Materials Engineering (SCME)

Dedications

I want to dedicate my work to all my respected **teachers,** and **colleagues,** my respected father **Zafar Iqbal,** mother **Abar-e-Saba,** father-in-law **Fayaz Ahmed Qazi,** and husband **Hamza Ahmed Qazi.**

Acknowledgments

Abstract

There has been considerable interest in the properties of nanosized mixed spinel ferrites from an application point of view in the last few years. They are used in gas sensors, energy storage, microwave absorption, television, modems, computers, and as radar-absorbing material at lower frequencies. Mixed spinel ferrites with regulated compositions, crystal shapes, and sizes can be synthesized. This allows researchers to customize their features for specific purposes. It is possible to fine-tune the magnetic and electrical properties of materials by altering their composition. In the present work single phase and nanosized Nickel Zinc Cobalt Ferrite with composition $Ni_xZn_xCo_{1-2x}Fe_2O_4$ (x = 0.0, 0.1, 0.175, 0.25) synthesized by chemical co-precipitation method. The prepared samples were calcined at 600 ^{0}C for 2 hours. The structural properties were investigated by XRD, SEM, and FT-IR instrumental techniques. The X-ray diffraction pattern confirms the formation of a single-phase cubic structure of the composition, $Ni_xZn_xCo_{1-2x}Fe_2O_4$ (x=0,0.1,0.175,0.25). The average crystallite size calculated by using the Scherer formula from the XRD data was in the range of 10-14 nm. SEM images confirmed the agglomerated structure of mixed spinel ferrite nanoparticles. The FTIR analysis was used to investigate the octahedral and tetrahedral band locations. An impedance analyzer was used to investigate the samples' dielectric properties. The dielectric studies revealed the enhancement of dielectric constant, dielectric loss, and tangent loss.   The AC impedance spectroscopy confirmed the resistance caused by the contribution of grain boundaries. The decreasing trend of impedance with the incorporation of Ni^{2+} and Zn^{2+} represents that conductivity increases in substituted samples which ultimately raise the absorption of EM waves. Using a vibrating sample magnetometer (VSM), the produced samples' saturation magnetization and coercivity were assessed. The saturation magnetization and coercivity values revealed a declining trend with increasing Ni and Zn content, according to the VSM study. The saturation magnetization at x=0.175 was increased to an ideal value of 73.49 emu/g. which makes it a potential candidate for EMI shielding applications in a high-frequency range.

Table of Contents

Table of figures

List of Tables

List of Abbreviations

M_s	Saturation magnetization
M_r	Remanence
H_c	Coercivity
SEM	Scanning electron microscopy
XRD	X-ray diffraction
VSM	Vibrating sample magnetometry.
FT-IR	Fourier transform infrared spectroscopy.
EDX	Energy dispersive spectroscopy
EMI	Electromagnetic interference
JCPDS	Joint committee of powder diffraction systems

Chapter #1

Introduction

1.1 Background of nanoscience and nanotechnology

The studies and applications of nanoscience and technology are embedded in the ideas of scientists. On December 29, 1959, at the California Institute of Technology in the Annualgeneral body meeting of the American Physical Society Richard P. Feynman. He delivered a great talk entitled 'There is plenty of roomat the bottom '. There, he conferred the objectives of engineering and managing objects at an atomic scale. He imagined the entire encyclopedia Britannica written on the head of a pin [1].

And after twenty years of this talk, many innovations and inventions started to emerge to defend Feynman's ideas. Technology consultants and foretellers understood the worth of these inventions and named this field Nanotechnology. Today we are using the devices that authorizeexactly what Feynman had predicted.

Drexler extended the ideas given by Richard Feynman in his famous book 'Engines of creation, the coming Age of Nanotechnology' [2]. Drexler gave some ideas about nanotechnology by saying'Nanotechnology is the atom-by-atom arrangement by controlling the structure of materials at themolecular level' through which, we can manufacture diverse nano machines. Althoughnano science and nanotechnology is a new word but naturally many processes were occurring at the micro and nanoscale from the start of life.

In 1974 the 'nanotechnology' term was first used by a Japanese 'Norio Taniguchi' in his paper ontechnology of creating objects on nano-meter scale. Then in 1986 an American engineer K. Eric Drexler used the term 'nanotechnology' in his book " the engines of creation: the coming era of Nanotechnology" [3]. Nanotechnology emerged as a field in 1980 by combination of theoretical and public (communal) work of Drexler. Drexler spread the conceptual framework of Nanotechnology.

The IBM scientist of Zurich invented the scanning tunnelling microscope in 1980 while the Gerd Binning and Heinrich Rohrer (Nobel prizewinners in 1986) developed microscope "Atomic Force Microscope" at IBM Zurich Research Laboratory through which materials can be seen at with extraordinary resolution up to atomic level.

In 1990 remarkable progress was made by IBM. The team of physicists said that they are going to use the 35 individual atoms of Xenon. And then in 1985 the new shapes of carbon molecules were discovered known as Buckyballs, which are spherical fullerenes, and it contains 60 carbon atoms. Then in 1991, after further progress carbon nanotubes were discovered. They are 200 times stronger than steel but just a sixth of its weight. They have excellent properties of thermal and electrical conductivities.

Further studies of semi-conductor nanocrystals led to the development of quantum dots. Their properties come both in bulk semiconductor and distinct molecules. Studying nanoscale characteristics, material synthesis, characterization methods, and application development are the main areas of interest in research.

1.2. Definition of Nano science And Nanotechnology

The term **nano** is originated from Greek word Dwarf. But scientifically 'nano' means one billionth.Thus, one nanometer is one billionth of a meter. E.g., the average diameter of human hair is 50,000nm. A human blood cell is approximately 2000 nanometers long.

Nano science is basically the study of composition and substances on nanoscale. When structures are manufactured at small scale on nanometer size range. Their properties become more attractiveand effective. Beam of electrons or ions are used by scientists to engrave properties as small as 25nanometers into metals, silicon and carbon-based materials [4].

Nanotechnology is the production of materials at the atomic level. The properties of materials change when the size of materials is reduced to the nano scale range. When particles are taken at nano scale then principles of classical mechanics are not able to describe the behavior (momentum, energy etc.) of materials at this small scale but quantum science is applied.

Nanotechnology is a field of integrated studies that is why it involves people from diverse fields including physicists, chemists, biologists, material scientists, engineers, and pharmacologists all together to work on

- Synthesis and manufacturing of nanomaterials and nanostructures and to study

the physicalproperties related to nanometer scale.

- To fabricate nano devices or devices having nanomaterials as their building blocks.
- To design and construct characterization tools for characterizing nanostructures andnanomaterials.

1.3. Fundamental Concepts in Nano science And Nanotechnology

Nano science and Nanotechnology has potential to view and manage atoms and molecules. Every single thing consists of atoms, the food, the garments, the buildings and houses and our bodies, everything is made up of atoms. Anything as small as atoms is impossible to see with the naked eye.

The recent nano science and nanotechnology are advanced nano-scale substances that were utilized for hundreds of years. Different sized silver and gold nanoparticles produced colors in shaded glass windows of antiquated church structures hundreds of years ago. The creators didn't know the materials they were producing surprisingly changed the formation of materials they were working on.

Scientists and engineers of this era are detecting a vast collection of methods to produce materialsat nanoscale to take control of the changed properties of these materials like excessive strength, low weight.

The particles between 1 and 100 nanometers in size are nanoparticles. In Nanotechnology a particle is defined as a small object that behaves as a whole unit with respect to its transport and properties [5].
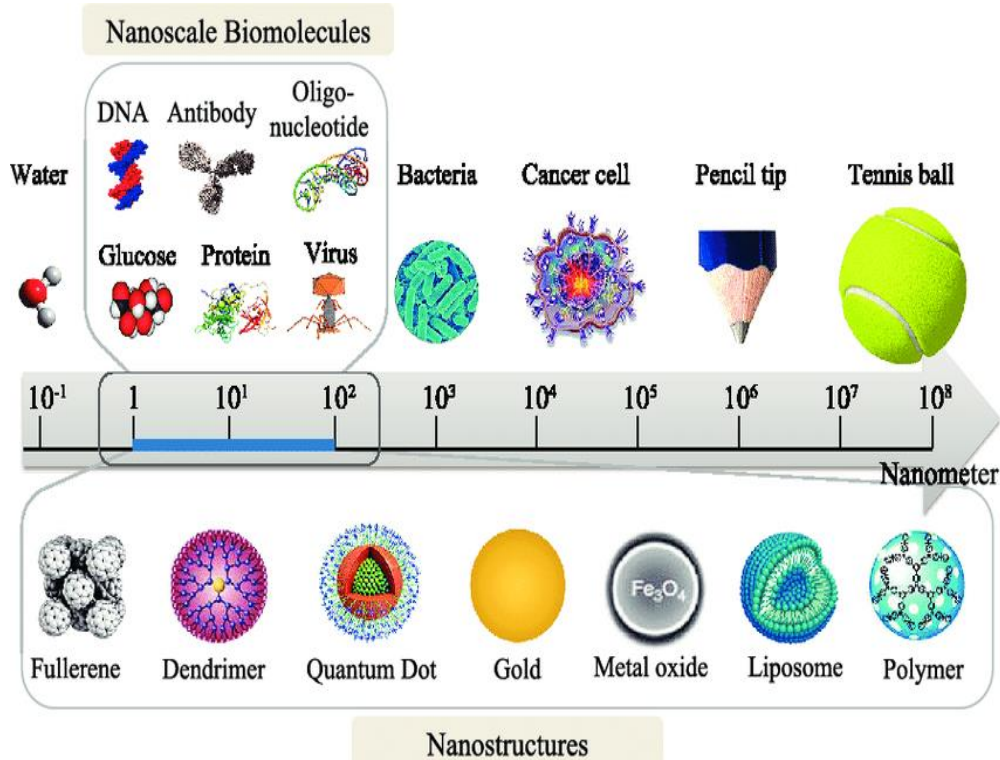
Figure 1 Nanoscale materials [2]

A nanoparticle (or Nano powder or nanocluster or nanocrystal) is a microscopic particle with at least one dimension less than 100 nm [6].

Due to vast range of prospective applications in optical, electronic, and biomedical field research on nanoparticles is the area of interest in the scientific probing. As nanoparticles are bridge between bulk materials and atomic or molecular structures.

As the size approaches the nanoscale and as the split of atoms on the surface of material becomesnotable the properties of materials changes. Nanoparticles shows distinct properties as compared to bulk materials. For example, Nanoparticles of copper less than 50 nm are excellent hard materials and they do not show the same ductility andsusceptibility.

Due to the small size of nanoparticles, they cause quantum effect by confining their electrons andthus show surprising properties. For example, nanoparticles of gold look deep red to black in solution. The surface area to volume ratio is high in nanoparticles. Thus, it shows immense diffusivity at high temperatures.

1.4. Magnetic materials and Ferrites

When magnetic field is applied to material, variation of internal and external flux

occurs and also the magnetization and magnetic induction vary in response to the applied magnetic field, based on such type of conduct materials can be categorize as follow [7].
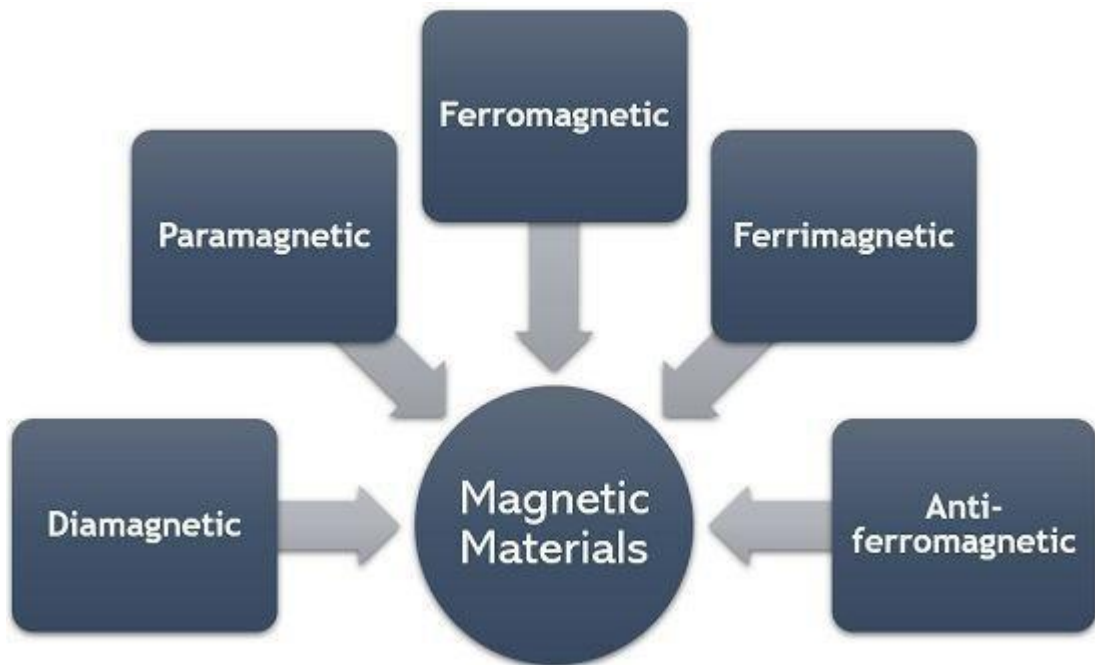
Figure 2 Types of magnetic materials

1.4.1. Diamagnetism

When material is subjected to magnetic field, diamagnetism behavior is observed owing to the motion of orbital of electron in that field. In this situation the net effect of magnetic moments of atom become zero thus has no internal magnetic interactions. An opposite field to the motion of orbital field is generated. Diamagnetic materials have the affinity to progress towards poor fields. In such type of materials, the external shells of their atoms are completely occupied.

1.4.2 Para magnetism

There is a permanent dipole moment in paramagnetic materials. The dipoles are arranged randomly canceling the magnetic effect of each other and show a zero-net magnetic effect on the material. On the subjection of external field to paramagnetic material, a torque is provided to the magnetic dipoles, and they align themselves in a proper direction i.e., dipoles & field have similar or dissimilar direction and in this way they get magnetized. But when the external magnetic field is detached then the aligned dipoles again loss their energy in no time and go back to their original random

positions and shows no magnetic properties again [8].

1.4.3 Ferromagnetism and Ferrimagnetism

There is permanent magnetic moment in ferromagnetic materials and show magnetization in the absence of an outer field. Mutual interaction of spin of domains creates the basis of this permanent magnetic moment in ferromagnetic materials. Domains have spins aligned in the same directions. Where the incomplete cancellation of dipole moment causes a lower permanent magnetization in ferrimagnetic materials. The sum of domain's magnetization makes up the macroscopic magnetization. Generally ferromagnetic materials are ionic solid i.e., they are electrically non-conductor whereas the ferrimagnetic materials are metals i.e. conductors [9].

Even in the absence of a field, ferromagnetic materials exhibit high magnetization due to the parallel alignment of their moment vectors. Ferromagnetism has two different properties.

- Spontaneous magnetization
- Magnetic ordering temperature
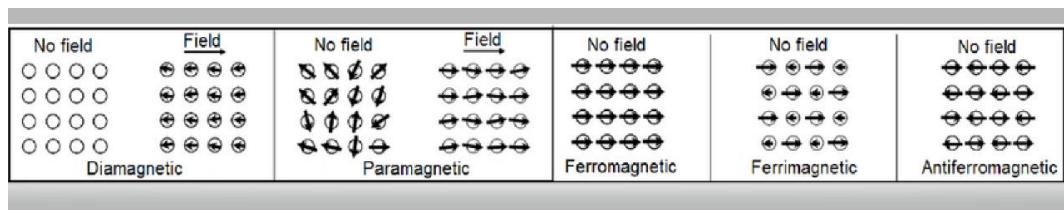
Figure 3 Order of dipole moments for magnetic materials

1.4.4 Anti ferromagnetic

Antiferromagnetic materials are analogous to ferromagnetic materials, but the difference exists when an antiferromagnetic material is subjected to in an external magnetic field, the atomic magnetic moment & external magnetic field become antiparallel to each other. In these materials the atomic magnetic moment of each atom is in opposite direction to other neighboring atom. So, they cancel each other effect and the net magnetization is zero in the absence of outer applied field of magnetic [10].

1.4.5 Super paramagnetic materials

Those materials which behaves as paramagnetic at temperature below the NEEL or Curie temperature. This phenomenon normally occurs in those materials which have very small size (crystallite of below 100nm) Because of this small size, the direction

of the entire crystallite can be easily altered regardless of whether the temperature is below the NEEL because very little thermal energy is needed for this activity. Hence there is tendency for the magnetic moment of entire crystallite to be changed instead of individual magnetic moment of each atom and this energy is called crystalline anisotropy energy. This energy depends on the crystallite size as the size of crystallite decrease this energy decreases accordingly [11].

1.5 Soft Ferrites

This category of ferrites is easily magnetizable and de-magnetizable. In the presence of a magneticfield, they take on the characteristics of a permanent magnet. They can be created through slow heating and cooling. Garnets, iron-silicon alloys, and ferrous-nickel alloys are a few examples of soft ferrites. They are utilized in the construction of electromagnets, computers, transformers, and other storage devices. The characteristics of soft ferrites are:

- A small hysteresis loop
- Minimal eddy current loss
- Little coercivity
- No contaminants or flaws
- Reduced magnetostatic energy
- An easier time building a domain wall
- High susceptibility and permeability
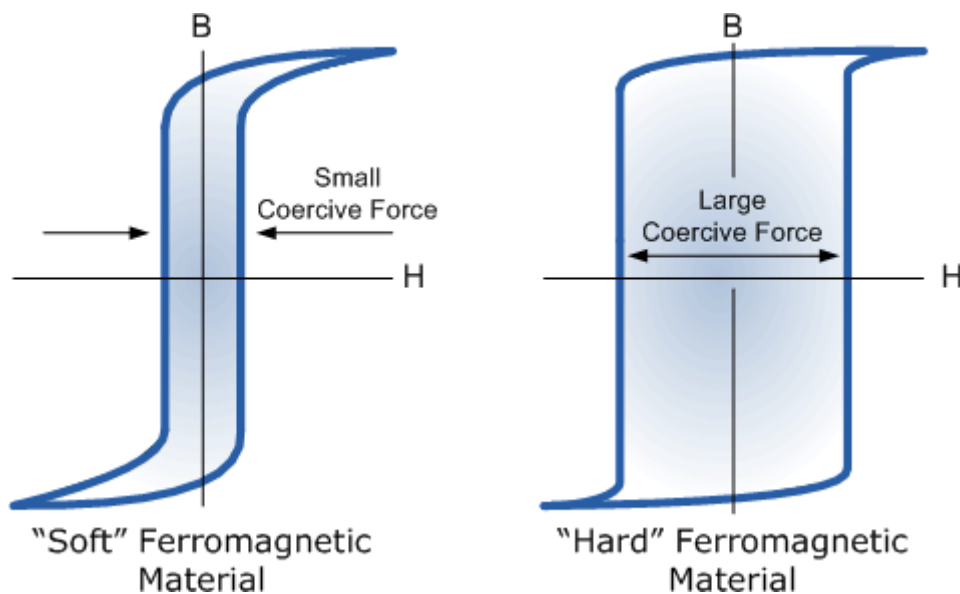
Figure 4 Hysteresis loops of Hard and Soft magnetic materials[12]

7

1.6 Hard ferrites

Magnetization and demagnetization are difficult processes for this category of ferrites, making them persistent magnets. The combination of a high temperature and a rapid drop in temperature creates them. Permanent magnets and direct current (DC) magnets are produced using these ferrites. Examples of these ferrites include Alnico, an iron-nickel-aluminum alloy, chromium, steel, carbon steel, and copper-nickel-cobalt alloys. Here are a few characteristics of hard ferrites:

- A large hysteresis loops.
- Impurities and flaws are more prevalent.
- There is high eddy current loss.
- There is high coercivity.
- Substantial magneto static.
- A challenging domain wall moment
- Low susceptibility and permeability

1.7 Ferrites and their structural classification

Ferrimagnetic materials or ferrite materials have partial abolition of the magnetic dipoles in a domain as result permanent magnetization of inferior strength is inherited; it is the summation of domains magnetizations. Generally non-conductive ferrimagnetic (ferrites) are ceramic compounds derived from iron oxides such as hematite (Fe_2O_3) or magnetite (Fe_3O_4) as well as oxides of other metals [7]. Based on the crystal structure and compositions, ferrites are classified as spinel, garnet and hexaferrite. In magnetic materials, ferrites which have broadly used practical applications in technology, have valuable attention. Ferrite nano particles among the magnetic materials are the most explorable magnetic materials. For sophisticated applications, they are used very expansively. It does not create unwanted eddy current in insulating material [13]. To increase the information density entered, it seems suitable for obtaining the Nano crystalline ferrites and to develop their based magnetic careers. Garnet, hexagonal and cube are three different structural directions in the ferrites: size and charge of metal ion are the determining factors of such structure, and these factors are also involved in balancing the charge of oxygen ions, and their relative amounts [13]. Since most of the ferrites are Spinel

and because of magnetic, electronic, optical, and catalytic properties, focus will be on Spinel ferrites [14].

1.7.1. Garnet

The common formula for garnet is $Me_3Fe_5O_{12}$. Me represents one of the rare earth metals. There are 8 formulae units or 160 atoms per unit cell of the cubic. There are 96 O_2 atoms spatially arranged with interstitial cations. An exceptional example of garnet is Yttrium iron garnet. The management of cations in garnet is quite intricate than the organization of cations in spinel, 24 Y^{3+} , 24 Fe^{3+} and 16 Fe^{3+} in decahedral site, in tetrahedral site ,in octahedral site respectively.
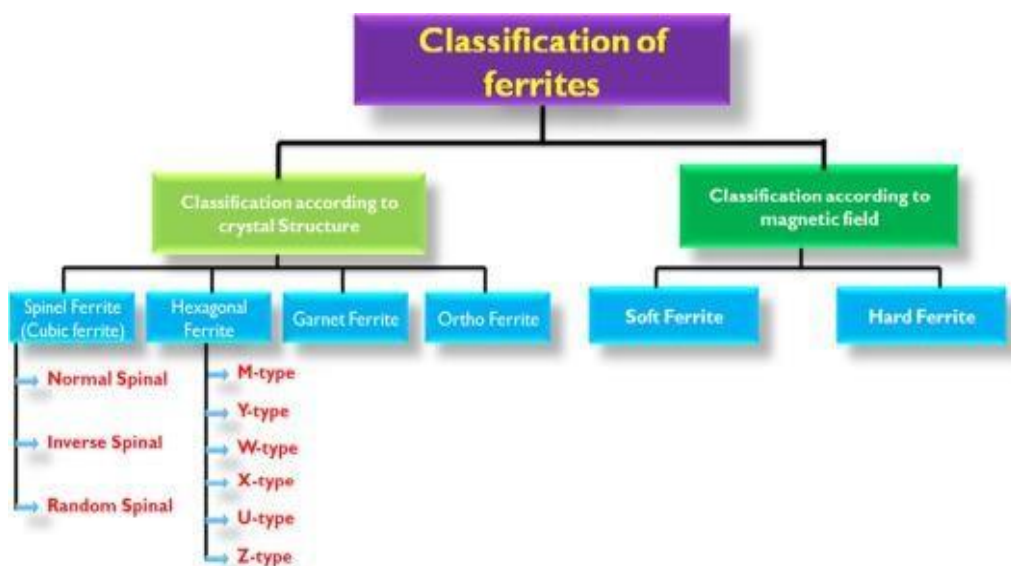
Figure 5 Classification of ferrites

Like the spinal and hexagonal ferrite, a wide range of transition metals can change Y^{3+} or Fe^{3+} ,in particular metals of rare earth can substitute the ions on decahedral and octahedral site. Other metal ions will be captured at decahedral, tetrahedral, and octahedral site. The Penta valent V^{5+} and divalent Ca^{2+} can be captured at tetrahedral and decahedral sites respectively.

1.7.2   Hexagonal Ferrite

It is used as a permanent magnet. It has very elevated coercivity [13]. The formula for hexagonalferrite is $MeO_6Fe_2O_3$ where Me corresponds to Ba, Sr, or Pb. The lattice of hexagonal ferrite is like the spinel structure in which oxygen is very tightly packed, but some metallic ions layers have equivalent ionic radii the same as oxygen ions. Three different sites in the lattice which are occupied by metal ions. These sites are octahedral site, trigonal site, and tetrahedral site.

1.7.3 Cubic Ferrite

All those materials which crystallize in spinel form or like that have common formula of AB_2O_4. A and B represent octahedral and tetrahedral sites while oxygen indicates anion site. Spinel ferrites have simpler structure as compared to the other ferrite types. The cubic structure of spinel is formed by 8 molecules of MeO and Fe_2O_3 with 32 anion sites of oxygen. Here Me is divalent cations. Cobalt (Co^{2+}), Copper (Cu^{2+}), Zinc (Zn^{2+}) and Nickel (Ni^{2+}) are the examples of divalent cations Oxygen ion form close face cubic structure. These sites (A and B) are partially filled with Fe^{3+} and Me^{2+} cation ions. Me^{2+} represents divalent cation. As per cation distributions, cubic structures are normally categorized as normal spinel, mixed spinel and inversed spinel. All these mentioned structures normally depend on choices of suitable order, whether it resides on A or it like to sit on B site. Table 1.1 show types of structures of some common metal ions of ferrites.

Table 1.1 Types of Ferrite's structure [11]

Type	Structure	General Formula	Example
Spinel Ferrites	Cubic	$A^{II}Fe_2O_4$	A^{II}=Cd,Co,Zn etc
Garnet	Cubic	$Ln_3^{III}Fe_5O_{12}$	Ln^{III} = Y,Eu etc
Hexagonal	Hexagonal	$A^{II}Fe_{12}O_9$	A^{II} = $BaF_{12}O_{19}$

1.7.4 Spinel Ferrites

These ferrites, which have the chemical formula $Fe_2O_4.M$ with a divalent cation as M, are magnetically soft. The metallic ions Mn, Mg, Ni, Co, and Zn are examples of post-transition metallic ions that can be M. To substitute Fe^{3+} ions, trivalent ions or a combination of divalent and tetravalent ions are utilized. They have two octahedral and tetrahedral crystallographic positions. They do not have preferred orientations of magnetization because of their cubic form. 32 tightly packed oxygen anions with 64 divalent tetrahedral sites and 32 trivalent octahedral sites make up each unit cell. Tetrahedral sites are where 8 cations and 16 cations are coordinated by 4 and 6 oxygen atoms, respectively (octahedral sites). Depending on the positive ion position,these ferrites are divided into normal, inverse, and mixed categories [15].

1.7.4.1. Kind of Spinel Ferrites

Categorization of Spinel structure is as:

- Normal spinel

- Inverse spinel

- Mixed spinel

A site is desirous by all the bivalent cations in normal structure of spinel [13]. The general formula for such a type of structure is Me^{2+} [Fe^{3+}] O_4^{2-}. Zinc ferrites have normal spinel structure Zn^{2+} [Fe^{3+}] O_4^{2-}. In Inverse spinel all divalent cation prefers to reside on B sites whileFe^{3+} contributes equally i.e., half on A site and half on B site. Fe^{3+} [$Me^{2+}Fe^{3+}$] O_2^{4-} is a general structure formula of such type of spinel structure. $NiFe_2O_4$ and $CoFe_2O_4$ are examples of inverse spinel structure. In these structures half of the Fe^{3+} resides on A site while the rest of Fe^{3+} ion rests on site B. The net magnetic moment is due to divalent cation of B site because due to Fe^{3+}cation on A and B they cancel each other moments.
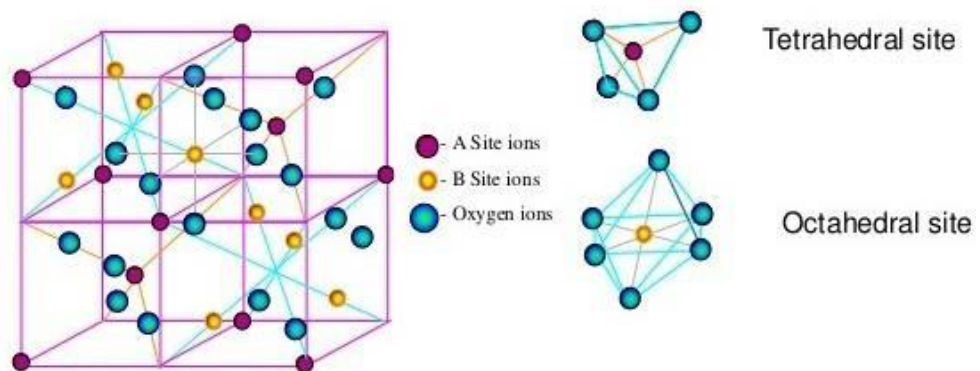
Figure 6 Crystal structure of spinel ferrites [16]

Table 1.2 Radii of some common cation employed in the spinel ferrites.

Ion	Ionic radii Å
Fe^{2+}	0.83
Fe^{3+}	0.67
Co^{2+}	0.82
Zn^{2+}	0.74
Ni^{2+}	0.78
Mn^{3+}	0.70

1.8 Applications of Ferrites

From the application point of view ferrites are alienated into two categories i.e., soft & hard ferrites. Here soft and hard do not mean their abrasiveness or penetration ability of material. If the material is magnetized and demagnetized very easily is called soft ferrite and if the material to be magnetized and demagnetized is not easy is termed as a hard ferrite. Soft materials are used for electromagnet purposes while for hard ferrites the most suitable application area is permanent magnet.

Some important characteristics like extensive utilization in today technology, their good electric resistivity at especially elevated frequency, Ferrite Nanoparticles has got the status of exceptionally critical magnetic materials [17]. Ferrite nanoparticles are used extensively owing to their following property.

- Inexpensive
- High Coercivity in ferrites
- Mechanical stiffness
- Time stability and useful temperature
- Usefulness at microwave frequencies
- Applications in High frequency area
- Broad range of materials

Ferrite nano materials are preferred due to the following reasons.

- High (>106 Ώ-cm) direct current electrical resistivity,
- Excellent magnetic properties,
- Chemically firm over ample temperature range
- Little eddy current losses.

Probable application areas are:

- Microwave devices
- Core Material
- Electromagnetic absorbers
- Drug delivery
- Ferro-fluids
- Data storage

1.9 Nickel Ferrite

Nickel ferrite is a type of soft magnetic material. Nickel ferrite nano particles having spinel nature are generally used in numeral electronics applications owing to their excellent permeability at elevated frequency. Other reasons for nickel ferrite nano particles in electronic application are that the electrical resistivity of nickel ferrite is amazingly high, mechanically nickel ferrite is very hard, chemically very stable, melting point is exceptionally low, specific heat is prominent, coefficient of expansion is good, magnetic moment saturation is low, magnetic transition temperature is low and available at very low cost in the market. Nickel has very strong inclination for tetrahedral site [18]. This makes Nickel ferrite inverse spinel structure. Nickel ferrite has cation distribution represented by $[Ni_{1-x} Fe_{1+x}] O_4$. Due to classical ferromagnetic properties of nickel ferrite, nickel ferrite among the soft magnetic material is one of the multipurpose and industrially central soft materials. Conductivity is low enough that results extremely low losses of eddy current, chemically high stable, catalytic behavior is good and abundance quantity in nature. For small particles size and for achieving unique properties have impelled the improvement of universally valid chemical approaches, including hydrothermal, Sono-chemical reaction sol-gel microwave plasma co-precipitation micro emulsion method citrate precursor method and mechanical alloying for the synthesis of chemically pure and stoichiometrically accurate spinel ferrite nano particles [18].

1.10 Cobalt Ferrites

Cobalt ferrite is a prominent material in EMI applications. It has attracted researchers due to so many useful applications in magnetic fluids, magnetic recording devices, high resistivity etc. Cobalt ferrite ($CoFe_2O_4$) has good chemical stability and excellent mechanical hardness. Cobalt ferrites are cubic ferrites. These have an inverse spinal structure. Where Fe^{3+} is sited at sites A and B Co^{2+} is located at B site. Cobalt ferrite has an anisotropy constant value from 1.8 to 3 x 106 erg/cm^3. The use of the cobalt ferrite in the magnetic recording devices must possess the high value of coercivity. High value of coercivity depends on particle size of the material. The size of particle near the critical size of the particle has the larger value of coercivity. The critical size is equivalent to the size of a single domain. Cobalt ferrite nanoparticles are extensively synthesized employing Co-precipitation process and sol-gel process are widely used for the synthesis of Fe (III) and Fe (II) salts are used for the synthesis of

the Nickel ferrite & cobalt ferrite nanoparticles. Cobalt ferrite was prepared by Blaskov (1996) synthesized by employing technique of coprecipitation. The calcination at 598 K was performed. The cobalt ferrite particles with diameter $50 \pm 5\text{Å}$ produced. XRD patterns showed that the lattice parameter is 8.20 Å and structure is cubic spinel. Cobalt ferrite ($CoFe_2O_4$) was prepared by Li (2006). The particle size obtained by Li was 10 to 15 nm. Moumen in 1995 produced the nanoparticles with diameter of 5 nm [19]. Pialli (1996) prepared the Cobalt ferrite ($CoFe_2O_4$) with diameter less than 50 nm. The dielectric property of the cobalt ferrite is of great concern. There are so many applications related to their electrical and dielectric properties. A lot of work has been done on these properties. Dielectric constant, dielectric loss, Ac and Dc electrical resistivity are very dependent on the crystal structure, grain size of the cobalt ferrite. The crystal structure and grain size depend on the process by which the material is formed. Enhanced Ac conductivity (σ_{ac}) is observed by amplifying the frequency. The dielectric loss is due to the imperfection and impurities in the crystal lattice. Enhancement in dielectric constant (ε') also increases on increasing the frequency. Amplifying frequency till 10 kHz, the dielectric constant value is improved. On further increase in frequency the decline in dielectric constant is observed. The explanation for the dielectric constant variation with frequency, is that the ferrites conversion from ferromagnetic to paramagnetic on varying the frequencies. The dielectric constant (ε') also changes with changing the temperature.

1.11 Zinc Ferrites

Numerous techniques have been used to synthesize zinc ferrite nanoparticles. Several ways could be used to characterize zinc ferrite. Magnetic spinel ferrites [M(II) Fe (III)$_2O_4$; M stands for Co, Mn, Ni, Zn, or Fe] nanoparticles have drawn a lot of attention from researchers in recent years due to their numerous technical applications in the domains of magnetic recording, microwave technology, catalysis, and biomedicine . $ZnFe_2O_4$ is a typical example of a spinel with usual structure. In addition, $ZnFe_2O_4$ has been used extensively in a variety of fields recently, including the hyperthermia treatment of cancer, as a semiconductor photo catalyst, as a gas sensor, as an absorbent material for the desulfurization of hot gases, as a component of composites, etc. A synergistic effect generated by the use of $ZnFe_2O_4$ nanoparticles (at a concentration of 100 μgmL^{-1}) in radiotherapy led to an approximately 17 times

increase in the effectiveness of cell death compared to that achieved by radiotherapy for highly radioresistant cancer cells. When water is exposed to sunlight, zinc ferrite can also be utilized as a catalyst to speed up the process (Fig. 7).[20]
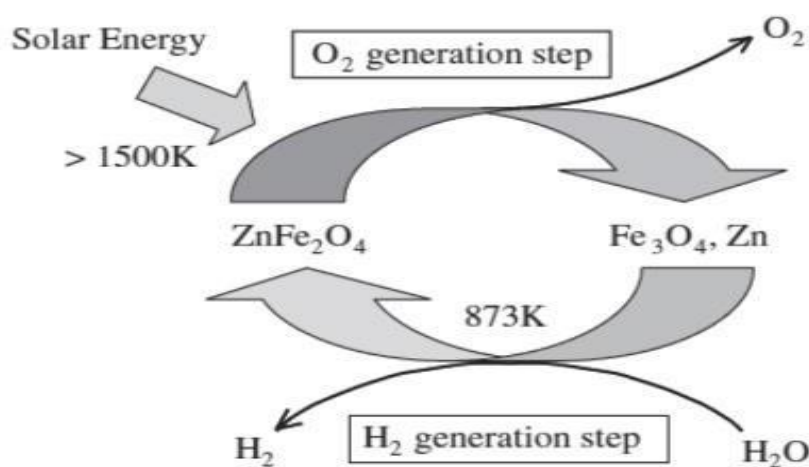
Figure 7 Schematic outline of two-step water splitting system with Zn ferrite.

The synthesis of Zn-ferrite nanoparticles of 2 to 12 nm size was done by a soft chemical coprecipitation method. The particle size was controlled by the pH of the solution. The XRD pattern of the synthesized samples showed single phase spinel structure. As d increases from 2 to 12 nm, the magnetization rises at 10 kg to 21.4 emu/g from 2.6 emu/g. For the sample with d=12 nm, the temperature dependent FMR studies display symmetric spectra with a single Lorentzian resonance peak. An extra peak of the main signal appears at the lower field side as the temperature drops. The antiferromagnetic (AFM) interactions between the ions in the tetrahedral and octahedral sites are shown by an increase in the g value and the linewidth (Hpp) with a reduction in temperature [21].

1.12 Dielectric properties

Ferrites have high activation energy which indicates their high resistivity at room temperature. This property of ferrites makes them suitable for applications as dielectric materials [22]. The dielectric materials are principally used as non-conducting materials. It is incredibly instructive to study electric field interaction with the atoms of dielectric materials. Polarization in dielectric materials takes place when materials are subjected to the field, polarization results owing to the occurrence of induced dipole moments, when the electric field is applied the cloud of electron move to one side resulting in the creation of dipoles which is

characterized by its dipole moments. In dielectric material each atom creates its small field, and this field interact with the field which is applied from the outside [23]. That process in which the negative charged electron cloud and positive ions of molecules or atoms are separated and then the dipole is oriented accordingly to the applied field or the disjointing of charge carriers which occurs at the border of grain boundaries upon the electric field subjection is termed as electric polarization [24]. Polarization is categorized in the following main four types.

- Electronic

- Ionic or atomic

- Dipolar

- Space-charge or Interfacial

Owing to the trapped and movable charges electric polarization is referred to space-charge polarization. This brand of polarization principally takes place in the polycrystalline and amorphous materials because in such type of material charge carrier like electrons, holes and ions are trapped on some sites and they get mobilize after getting some energy. The mechanism which is responsible for the transportation is defined by knowing the dielectric behavior of a material. Permittivity or relative permittivity is the most important property of a dielectric material in which generally the dielectric constant property of a dielectric material is discussed. The following factors manipulate the dielectric permittivity.

- Frequency of alternating electric field
- Rate of change of time-varying field
- Chemical structure of dielectric material
- Imperfections (defects) of the material
- Physical parameters like pressure, temperature etc.

The dielectric constant and the frequency of the applied external field both depend on each other. The dielectric polarization fluctuates accordingly to the fluctuation of external field, but the polarization does not catch the variation speed of applied field, there is constantly a lag between them. Decrease in dielectric polarization occurs if it does not follow the speed at which external field variate. The polarizations track the fluctuations of the field when a field of low frequency is applied and hence in that case the dielectric constant remains almost unchanged. In

case when the fields applied is of high frequency the polarization cannot catch the speed of variable field and its dielectric constant starts to decrease and at one stage when the frequency reach to very high value then the orientation polarization stops due to relaxation of dielectric materials [23]. Due to the low dielectric constant, high electrical resistivity and dielectric losses, spinel ferrites are very good candidates for the microwave's absorptions and other EMI applications.

1.13   Objectives

The objective of this study is to

- Synthesize the nanoparticles of Nickel Zinc Substituted Cobalt Ferrite with different compositions by an easy and affordable method called co-precipitation.

- Characterize these nanoparticles for structural, electrical, and magnetic properties.

- To investigate the effect of nickel and zinc substitution on cobalt ferrite for electromagnetic interference shielding.

Chapter#2

Synthesis Techniques and Methodologies

2.1. Literature Review

Many technological applications and their flexible use have made ferrite nanoparticles a topic of research. For this purpose, ferrite properties have been developed day by day. The results of workdone on a few of them are listed below.

S.Sathiya prepared nano-size $CoFe_2O_4$ ferrite by a technique of Co-precipitation. X-ray diffraction & Scanning Electron Microscope were used for the characterization of resulting powders showing nano-size particles. The XRD data and FTIR data confirm the spinel structure of cobalt ferrite [25]

A series of Al substituted nickel ferrite nanoparticles, synthesized by Coprecipitation and sol-gel technique [26]. The X-ray diffraction (XRD) patterns of all the samples confirm that a spinel structure has formed and that the size of the crystallites is between 25.4 $\pm$3 nm. FTIR measurements showed that there were two basic absorption bands, which were given to tetrahedral and octahedral sites. The DC electrical resistivity measurement reveals that it increases if the concentration of Al^{3+} increases. Also, it was observed that the Tan loss and dielectric constant decrease as the concentration of Al^{3+} are increased by **I.H Gul** and **Erum Pervez**.

L P S Sagala, S Humaid and **K Tarigan** studied the magnetic properties of $Zn_{0.7}Ni_{0.15}Cu_{0.15}Fe_2O_4$ by coprecipitation method at 100 $^\circ$C. these nanoparticles were characterized by XRD, FESEM, EDAX.XRD results confirm that spinel ferrites were of cubic shape and the crystallite size was 14.5087 nm. The FESEM result showed that nanoparticles were spherical and agglomerated. Magnetic hysteresis showed that $Zn_{0.7}Ni_{0.15}Cu_{0.15}Fe_2O_4$ was soft magnetic [27].

Sadaf Bashir Khan and **Shern-Long Lee** synthesized nickel zinc ferrite by coprecipitation method with different stoichiometric proportions. The prepared samples were then characterized by XRD, SEM and FTIR. XRD patterns showed cubic spinel ferrites the particle size was in the range of 20-60 nm. The overall results shows as Zn substitution in Ni Zn nano ferrites grows, the lattice constant a_0 rises while the crystalline strain falls [28].

Mohammad A. Ati and **Hayder Khudhair** studied Cobalt doped Nickel ferrite by

Coprecipitation method. From the diffraction of X-ray's study, single phase and inverse spinel from the obtained powders is revealed. The size of grain was calculated from data of XRD, was inveterate by Field Emission Scanning Electron Microscope and photograph obtained confirm nano size particle of the cobalt doped nickel ferrite. The effect of cobalt larger ionic radius, i.e., increased from 16 to 19nm was also noticed that the crystallite size increases as the concentration of cobalt increases. FTIR data showing the vibrational bands confirm the spinel structure of the ferrite nano particle [29].

$(Ni_xFe_{3-x}O_4)$ were synthesized by **Mahalakshmi et al**. They noted a drop in dielectric values and an increase in dielectric loss values. The study also demonstrated that ac conductivity is influenced by nickel concentration since it isn't just reliant on electron transfer between Fe^{2+}/Fe^{3+} ions but also on Ni^{2+}/Ni^{3+} ions. Increasing frequency also enhanced conductivity values [30].

The electrical, magnetic, and structural characteristics of nickel as well as the composite of nickelferrite with transition metals and rare earth metals were examined by **Y.C. Yang et al.** The properties were compared after using the sol-gel and co-precipitation methods. By using the solution-gel approach, large-scale ferromagnetic particles with many domains and high resistancewere created. The particles can be applied in high frequency applications. The particles created by the co-precipitation approach had a single domain, were paramagnetic, and were reduced in size. The particles were used in magnetic resonance imaging, drug delivery, and other fields of medicine, among others. It was found that doping nickel with rare earth elements lowered magnetization. When transition metal was added, the coercivity rose. When rare earth metal ions were doped, dielectric loss was reduced. Particle size increased as transition elements were doped. Doping also led to an increase in the lattice constant. It was seen that the unit cell was expanding. By doping with transition metals, it was seen that the dielectric loss of doped nickel ferrite decreased and the resistivity increased [31].

A.E. Paladino et al. studied microwave properties of ferrites. The subject of the investigation washigh peak power fine grain nickel ferrite. Through hot press ball milling, ferrite nanoparticles werecreated, and flame spraying was used to create composites. The finding was that as particle size dropped, absorbance increased, and dielectric loss also decreased. With composition, the dielectriclosses provided by low

field also decreased. In fields with greater thresholds, cobalt was used instead. The 750 KW power level was used with the prepared fine-grained ferrite that was also hot pressed. Nonetheless, a nonlinear behavior was noted below 20 kW of peak power [32].

Nickel ferrite was created by **Shanmugavel et al.** There was a 1:1 ratio. Several techniques wereeffectively used to observe the micro characteristics of structures and other measurements of nano [33].

L P S Sagala, S Humaidi, K Tarigan. et al. carried out research to check the nanostructure and magnetic properties of the synthesized $Zn_{0.7}Ni_{0.15}Cu_{0.15}Fe_2O_4$ nanoparticles. Co- precipitation method was used to synthesize these nanoparticles. Then these nanoparticles of sample were characterized by XRD, FE-SEM, EDAX. The VSM was also done for the magnetic property of the sample. The hysteresis loop showed that the synthesized material was soft magnet [27].

Using the sol-gel combustion approach, **Minakshi arya, Mayuri N. Gandhi and Siddhartha P Duttagupta** created $Ni_{0.5}Co_{0.2}Zn_{0.3}Fe_2O_4$ nanoparticles with success. The sample's single-phase formation and polycrystalline makeup were both validated by the XRD examination. The sample's micro- and nanoscale morphologies were revealed by FE-SEM and FE-TEM investigations, respectively. A broadband dielectric spectrometer was used to measure the sample's complex dielectric constant, which came out to be 11.05-j1.03 at 1 MHz The complex optical conductivity of the sample is 17.40-j27.54 S/m in the frequency range of 0.3 - 2.2 THz at room temperature, and the complex refractive index of the sample is practically constant at 3.30-j0.03 and 10.88-j0.23, respectively. At a temperature between 300 and 50 K, the MH hysteresis curves showed low coercivity and high saturation magnetization ranging from 2.81 to 96.80 Oe and 85.60 to 95.00 emu/g, respectively. $Ni_{0.5}Co_{0.2}Zn_{0.3}Fe_2O_4$ nanoparticles may be a viable material for RF/THz frequency-selective surface applications due to their noticeably high dielectric constant values and low losses (0.09 at 1 MHz and 0.02 at 0.3–2.2 THz) [34].

By using the Sol-Gel method, $Ni_{0.6-x}Zn_{0.4}Co_xFe_2O_4$ (at x=0) and $Ni_{0.6-x}Zn_{0.4}Co_xFe_2O_4$ (x=0.011) were effectively synthesized by **Rajinder Kumar, Ragini Raj Singh and P. B. Barman**. The development of nanocrystalline materials is demonstrated by XRD measurements. According to the most prominent peak (113) of the XRD diffraction pattern, the crystallite sizes of $Ni_{0.6-x}Zn_{0.4}Co_xFe_2O_4$ (at x=0) and $Ni_{0.6-x}Zn_{0.4}Co_xFe_2O_4$

(x=0.011) were found to be 23 nm and 24 nm, respectively. Co doping is required to change structural characteristics such d-spacing, lattice constant, strain, dislocation density, and packing percentage. These values were estimated using XRD peaks [35]. **Ninad B. Velhal, Narayan D. Patil** and **Vijaya R. Puri** concluded in their paper that, the simple and low temperature auto-combustion method proved successful in producing $Co_{1-x}Ni_xFe_2O_4$. The development of cubic spinel phase with modest reflections of Fe_2O_3 phase is visible in the X-ray diffraction pattern. The biggest crystallite size, 44 nm, and maximum magnetic moment, 92.86 emu/gm, are found in the 0.4 Ni substituted cobalt ferrite. These results are greater than the earlier reported value 21 using the aerosol method, suggesting that the auto combustion technique may be a better synthesis method. As conductivity increases as frequency increases, the dielectric constant and loss tangent both decreases. Due to nickel's lower magnetic moment, the magnetic characteristics show that as the Ni content rises, the M_s, M_r, H_c, and M_r/M_s decrease. Moreover, the behavior of magnetic characteristics is temperature dependent. With increasing temperature, the values of M_s, M_r, H_c, and M_r/M_s drop [36].

By using the co-precipitation process and citrate as a chelating agent, nickel cobalt ferrite ($Ni_{1-x}Co_xFe_2O_4$; x = 0.3, 0.5, 0.7) was created and described by **S. R. Gibin** and **P. Sivagurunat**. It was then calcined at various temperatures, including 400, 600, and 800 °C. The generated sample was nanosized and well crystalline nickel cobalt ferrite nanoparticles, according to the XRD pattern. By TG/DT analysis, the mechanism of $Ni_{1-x}Co_xFe_2O_4$ nanoparticle generation was investigated. This research also validated the necessity of calcination. Using FESEM and FETEM with SAED method, the produced nanoparticles' cubic form was determined. The elemental makeup of the synthesized chemical (Ni, Co, and Fe) was shown by EDAX analysis to be in the proper proportions. The particle size determined from XRD was computed using the Debye Scherer formula, which corresponds well with the particle size determined from FETEM using the software "image j viewer." The higher capacitance of 865 Fg^{-1} ($Ni_{0.5}Co_{0.5}Fe_2O_4$) at the slower scanning rate of 2 mV s^{-1} provided a clear indication of the potential suitability of the produced nanoparticles for super capacitance applications. It is possible to infer from the XPS analysis that the $Ni_{1-x}Co_xFe_2O_4$ nanoparticles have existed in several oxidation states. DLS Zeta Potential study verified the produced nickel cobalt ferrite nanoparticle's improved stability [37].

Crystalline nanoscale characteristics of Zinc, Nickel Was compared by **Manju Kurian and Divya S. Nair** the production of ferrite particles made by co-precipitation and sol-gel auto combustion. The resulting particles were discovered to have cubic spinel structure and range in size from 17 to 40 nm. The development of ferrites was confirmed by the FTIR spectra's detected peaks. The tetrahedral (A) and octahedral (B) interstitial sites in the spinel lattice are where the two primary absorption bands, the high frequency band m_1 around 600 cm^{-1} and the low frequency band m_2 around 400 cm $^{-1}$, respectively, originate. Also, it was discovered that, with the exception of the SGE sample, the temperature had little bearing on how the ferrite samples aggregate. The XRD measurements and TEM images are consistent. This study showed that one of the easiest and most efficient chemical methods for producing ferrite nanoparticles is the sol-gel combustion process.[38] .

Ionic radii have a significant impact on the size of crystallite nano ferrite particles, according to research by **Gangothri S. Kumar**. Cobalt-replacement nickel ferrite was created using the sol-gel method. The x-ray diffraction technique was used to characterize the synthesized nano particle. Incorporating nickel into cobalt ferrite reduces the crystallite size of the nano particle because nickel has a lower ionic radius than cobalt. The spinel structure of the ferrite nanoparticle, as shown by FTIR and Raman Spectroscopy, is preserved by the inclusion of nickel ion into the cobalt ferrite [39].

2.2 Synthesis and Experimentation

Nanomaterials can be in one dimension (e.g., nanowires, nanotubes), two dimensions (e.g., thin films), and three dimensions (bulk materials). Nanomaterials can be in agglomerates, single, fused, and aggregated forms with many different shapes e.g., spherical, tube shaped and improper shapes/irregular shapes. Quantum dots, fullerenes and nanotubes are the most ordinary types of nanomaterials.

Nanomaterials are those materials which meet at least one of the following criteria:

- Consist of particles with one or more dimensions in the size range of 1-100 nm for morethan 1% of their number.

- Internal or surface structures in one or more dimensions must be in size range of 1-100 nm.

- Specific surface to volume ratio >60 m^2/cm^3 excluding materials having particle size lessthan 1 nm.

Nanomaterials are classified into four categories [40]:

- 0-D: Length, breadth and heights are confined at single point (e.g., nano dots).

- 1-D: It has only one parameter, either length or breadth or height (e.g., very thin surfacecoatings).

- 2-D: It has only length and breadth (e.g., nanowires, nanotubes)

- 3-D: It has all parameters of length, breadth, and height. (e.g., nanoparticles)
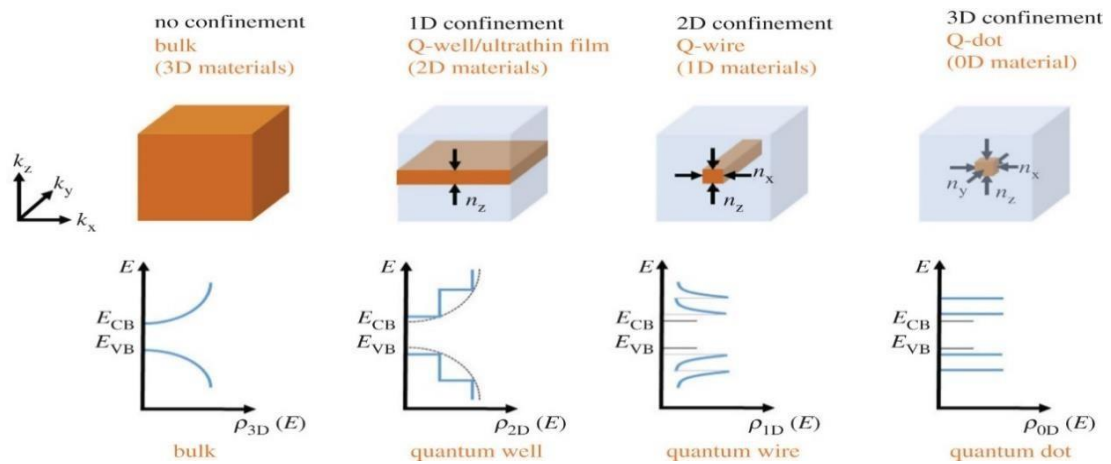
Figure 8 Nanomaterials in different dimensions.

2.3 Fabrication Techniques for Nanomaterials

Every synthesized nanomaterial have its own significance related to the specific application [41]. Thus, the manufacturing of nanomaterials with modified characteristics includes the control of size, shape, structure, composition, and purity of the substance.

Formation of nanomaterials by the mixing of two or more substances together is called synthesis of nanomaterials. Techniques used for fabrication of nanomaterials are called synthesis techniques for nanomaterials. Generally, there are two types of approaches for the synthesis and fabrication of nanomaterials and nanostructures.

- Top-down approach
- Bottom-up approach
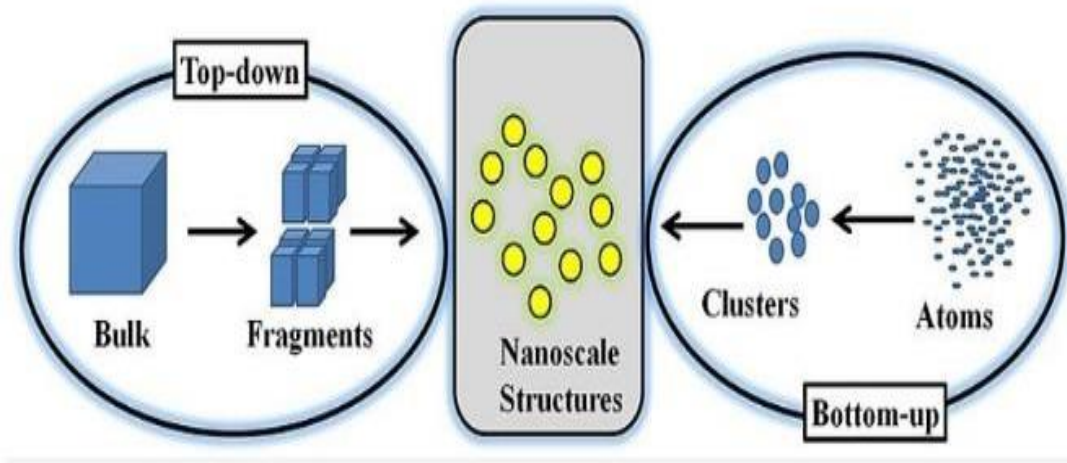
Figure 9 Illustration of Top-down and Bottom-up approach for fabricating Nanoparticles [42]

The cutting and slicing of bulk material into nanosized particles are called **the top-down approach.** There are two types: attrition and milling. Devices that self-assemble are said to "make themselves" using **bottom-up processes**. One illustration is the creation of chemicals. Although having control over the processes is challenging when objects become larger and bulkier than what is typically generated via chemical synthesis, bottom-up methods should be able to produce devices in parallel and considerably cheaper than top-down approaches. Nature, of course, has had plenty of time to develop and perfect the wonder-working self-assembling mechanisms. Nanomaterials can be synthesized by both physical and chemical methods.

Physicochemical Methods

- Laser Ablation
- Ultraviolet Irradiation
- Lithography
- Photochemical Reduction
- Sonication
- Milling

- Aerosol Technology
- Electro-chemical
- Emulsification
- Molecular
- Spray Pyrolysis
- Vapour Deposition

- Polymerization
- Dialysis
- Solvent diffusion
- Atomic Condensation
- Sol-Gel Process

Bulk material

4 Au NPs

Oxidizing agent

Reducing agent

Au NPs

AuCl

(b) Top-Down Approach

Synthesis of Metallic Nanoparticles

Bottom-up Approach **(a)**

- Microbial synthesis
- Phyto-synthesis
- Use of biological extracts
- Synthetic biology and biotechnology

Biological Methods

Figure 10 (a) Bottom-up and (b) Top-down approaches for synthesis of metallic nanoparticles using conventional physicochemical and relatively new eco-friendly biological methods [43]

- Co- Precipitation method
- Sol-gel
- Hydrothermal
- Solvothermal
- Microemulsion

2.4. Sol-gel Method

The sol-gel method is based on the spontaneous production of a dual phase material (gel) from a solution (sol) containing inorganic precursors and stabilizing agents via hydrolysis and condensation. The evaporation of the solvent drives additional gel phase change, resulting in the development of xerogel phase. When the xerogel is dried, the solvent molecules are totally removed, resulting in additional aggregation of inorganic clusters and the production of solid materials.

2.4.1. **Advantages**

- This technique is incredibly easy and economical.
- Sol Gel guarantees a high degree of purity.
- Because stirring is ongoing, excellent homogeneity is resulted.
- The process uses relatively low temperatures.
- This technique has wide applications in electronics, optics, and energy.

2.4.2. **Disadvantages**

- Poor bonding.
- Controlling porosity is quite challenging.

2.5. Microemulsion Method

Using a chemical process, two phases are combined in this method. Metal salts and surfactants make up the aqueous phases, while another phase could be water or oil. Micro emulsions come in two varieties: direct and reverse. In the former, oil is dispersed in water, whereas in the latter, water is dispersed in oil.

2.5.1. **Advantages**

- The distribution of pore sizes is favorable.

2.5.2. **Disadvantages**

- The surfactant is challenging to remove.

2.6. Solvothermal or Hydrothermal

Appropriate temperature and pressure are necessary for chemical reactions to occur. The precursor is mixed with the solvent in sealed jars that are heated to a temperature above the boiling point of the solvent. If water is used, the process is referred to as hydrothermal, and if another solvent is used, it is referred to as solvothermal.

2.6.1. **Advantages**

- By adjusting time, temperature, solvent concentration, and type, morphology can be controlled simply and precisely.
- It is quite a simple method.

2.6.2. **Disadvantages**

- Unsafe.
- Expensive autoclaves and reactors.

2.7. Co-precipitation Method:

Co-precipitation is the method carried down by precipitates of substance normally soluble under the conditions specified. In this method the metal cations involved from a conventional medium are co-precipitated generally as carbonates, oxalates, hydroxides. These precipitates are then heated/ calcined at suitable temperature to produce the final powder. For high uniformity/ homogeneity. the soluble products of the precipitates of metal cations must be adjacent. This process then results ion atomic scale mixing and therefore the low temperatures is required for heating for the formation of final product [44]. Which gives low particle size. Though every synthesis needs its own specific conditions, precursor reactions. And this process also needs to control the pH, temperature solution concentration and the stirring speed of mixture to yield the final product with specific properties.

Trace elements are concentrated and separated from diluted solutions like natural water by co-precipitation method. Control of pH is necessary for an effective co-precipitation of metals [45]. Co-precipitation is a chemical wet method in which fine nanoparticles are obtained; it is also used   for the preparation of fine, pure and homogenous nanoparticles of ferrites.
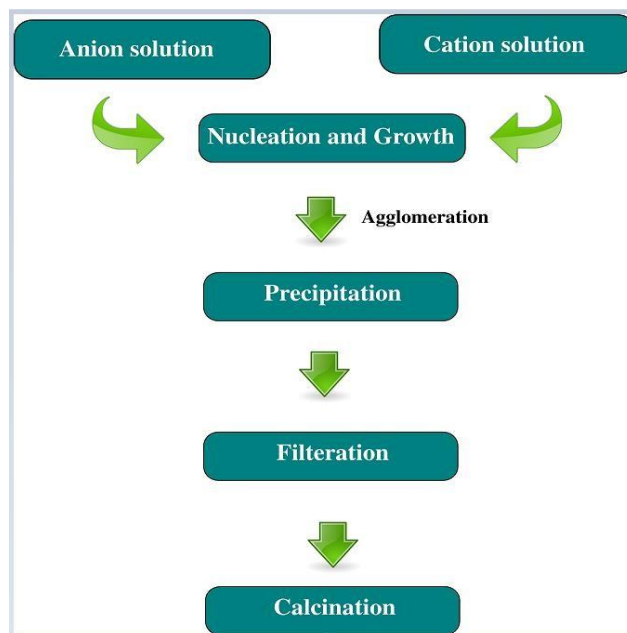
Figure 11 Illustration of Co-precipitation method used for synthesis of magnetic nanoparticles [46].

2.7.1. Advantages of Co-precipitation Method:

- Cost effective method.

- No need of a high temperature.
- Consistent and large-scale fabrication
- Useful for the production/fabrication of metal oxides.

This technique is more useful as compared to any other techniques due to its various advantages such as simple to handle, cost effective, no need of high temperature, consistent and large-scale fabrication.

2.8. Synthesis of Mixed Spinel Ferrite:

The synthesis of nanoparticles can be done by various techniques like Co-precipitation, sol gel method, hydrothermal method and solvothermal method. Here we have synthesized different compositions of $Ni_xZn_xCo_{1-2x}Fe_2O_4$ by co-precipitation method. The co-precipitation process is a crucial step in the creation of nanoparticles. The product obtained is highly pure. The following stochiometric formula was used to determine mass for various chemical compositions employed in the process:

Mass = (molarity x molecular weight x 200 ml) / 1000)

2.8.1. Synthesis of Cobalt Ferrite:

Here $CoFe_2O_4$ nanoparticles were prepared by co-precipitation method. In this method the metal cations from conventional medium are co-precipitated generally as hydroxides, oxalates, and carbonates. Then the formed precipitates are eventually heated/calcined at proper/desired temperature to produce the final powder. The starting materials for the reaction were cobalt nitrate $(Co(NO_3)_2.6H_2O)$ and iron nitrate (III) nonahydrate $(Fe(NO_3)_3.9H_2O)$ provided by EMSURE® Merck KGaA Darmstadt Germany (99% purity), sodium hydroxide (NaOH) provided by Fischer Chemical Ltd. All the materials were analytical grade. Cobalt nitrate, sodium hydroxide (3M) and iron nitrate were dissolved in stoichiometric amount in 200 ml of deionized water. Each solution was magnetically stirred for ten minutes. Deionized water was used as a solvent to minimize the presence of impurities in the final product. The solutions of cobalt nitrate and iron nitrate were mixed together and magnetically stirred for 30 minutes at room temperature for homogenous mixing. The nitrates solution was heated under constant stirring up to 80-85 °C. The solution of precipitating reagent, already heated at 80 °C, was mixed with the nitrates solution under constant stirring at the temperature of 85 °C. Both solutions were heated at 85 °C for 45 minutes under constant stirring. Deionized water was used for thoroughly washing the precipitates in order to obtain impurity free cobalt ferrite nanoparticles. The water content was removed by drying the product in

electric oven overnight at the temperature of 80 °C. The dried product was grinded into fine particles and calcinated in muffle furnace for two hours at 600 °C.

2.8.2. Synthesis of $Ni_xZn_xCo_{1-2x}Fe_2O_4$ (x = 0.1, 0.175, 0.25):

The starting materials for the reaction were cobalt nitrate ($Co(NO_3)_2.6H_2O$), Nickel nitrate ($Ni(NO_3)_3$). $6H_2O$, Zinc nitrate ($Zn(NO_3)_3$).$6H_2O$ and iron nitrate (III) nonahydrate ($Fe(NO_3)_3.9H_2O$) provided by EMSURE® Merck KGaA Darmstadt Germany (99% purity), sodium hydroxide (NaOH) provided by Sigma Aldrich. Cobalt nitrate, Nickel nitrate, Zinc nitrate, sodium hydroxide (3M) and iron nitrate each were dissolved in stoichiometric amount in 200 ml of deionized water. Each solution was magnetically stirred for ten minutes. Deionized water was used as a solvent to minimize the presence of impurities in the final product. The solutions of cobalt nitrate, Nickel nitrate, Zinc nitrate and iron nitrate were mixed and magnetically stirred for 30 minutes at room temperature for homogenous mixing. The nitrates solution was heated under constant stirring up to 80-85 °C. The solution of precipitating reagent, already heated at 80 °C, was mixed with the nitrates solution under constant stirring at the temperature of 85 °C. Both solutions were heated at 85 °C for 45 minutes under constant stirring. Deionized water was used for thoroughly washing the precipitates to obtain impurity free cobalt ferrite nanoparticles. The water content was removed by drying the product in electric oven overnight at the temperature of 80 °C. The dried product was ground into fine homogeneous particles with help of mortar and pestle and calcinated in muffle furnace for seven hours at 600 °C. Three different samples (x = 0.1, 0.175, 0.25) were prepared following this method.
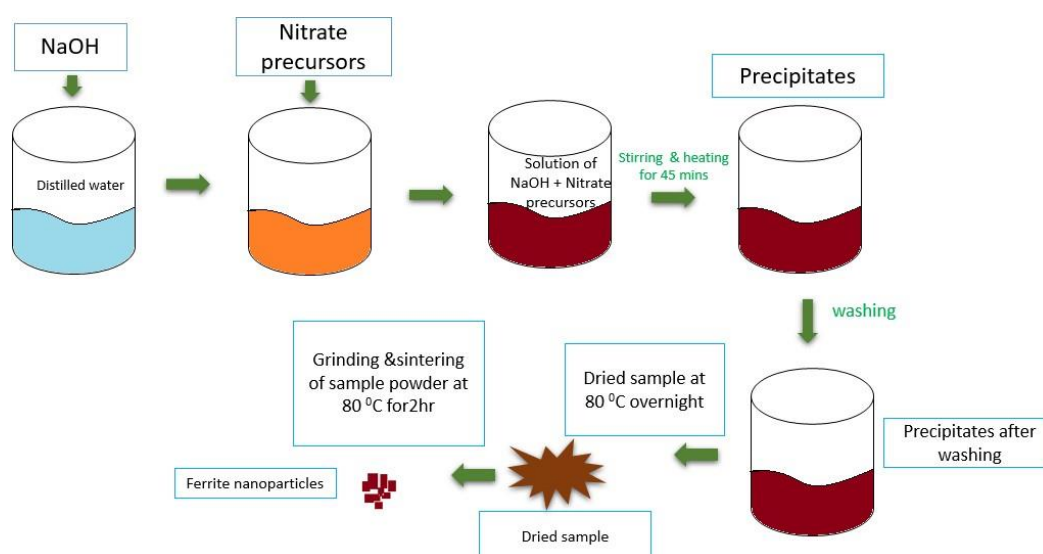
Figure 12 Pictorial representation of synthesis method used for developing ($Ni_xZn_xCo_{1-2x}$ Fe_2O_4) nanoparticles.

2.9. Testing Sample Preparation

The following is a discussion of the various techniques used to prepare samples for the measurement of SEM, FTIR, electric, and magnetic properties:

2.9.1. Sample preparation for FTIR

The die was filled with ground KBr and the small amount of sample after which it was placed in the hydraulic press system at 3 tons for nearly 15 seconds. Pressure was released and the die was removed after 15 seconds. In the end, a thin sample pellet with a thickness of 2-3 mm and adiameter of about 13 mm lateral size was produced and used for FTIR testing.

2.9.2. Sample preparation for SEM/EDS

The powdered substance was sonicated for two hours after being dissolved in DI water in a very little volume. After being poured onto a spotless glass slide, the mixture was dried in the oven for an hour before being utilized for SEM/EDS analysis.

2.9.3. Sample preparation for electrical properties

Using hydraulic press equipment and five tons of pressure for five minutes, each sample (1gram) was finely ground to create pellets with a 13mm diameter. Following preparation, the pellets were sintered in a furnace for three hours at 550 °C. Each pellet's thickness was determined using a vernier caliper, and the results were used to calculate its permittivity, dielectric constant, and other electrical properties.

Chapter # 3

Characterization Techniques

Some specialized scientific approaches can be used to analyze the various properties of synthesized Cobalt Nickel Zinc ferrite nanoparticles (x = 0, 0.1, 0.175, 0.25). One of the approaches can be used to collect physical or chemical properties as well as information about the material such as phase, structure, morphology, lattice parameter, crystallite size, and so on. This chapter will briefly explore the following characterization strategies.

Characterization techniques are used to characterize the synthesized samples. To analyze whether the desired particles are formed or not. These characterization techniques provide us the opportunity to study the behavior and properties of synthesized material at the nanoscale.

3.1. Characterization techniques used:

- XRD (X-ray diffraction)

- FTIR (Fourier transform infrared spectroscopy)

- SEM (Scanning electron microscopy)

- VSM (Vibrating sample magnetometer)

- Dielectric properties

3.2. X-ray Diffraction Technique:

It is a valuable instrument for determining the degree of crystallinity and the structure of a material. XRD can provide detailed information regarding structural strain, crystal flaws, average crystallite size, crystallographic orientation, and degree of crystallinity. There are three ways for determining crystal structure: powder diffraction, Laue method, and rotating crystal method. If the powder diffraction method is used, two ways can be used to calculate crystal size. These methods are as follows.

1. Debye Scherrer Technique

2. Diffractometer technique

The sample was ground into a fine powder. Copper, Molybdenum, and other metals can be employed as targets. The Cu-k alpha=1.54 source was employed for analysis in this case.
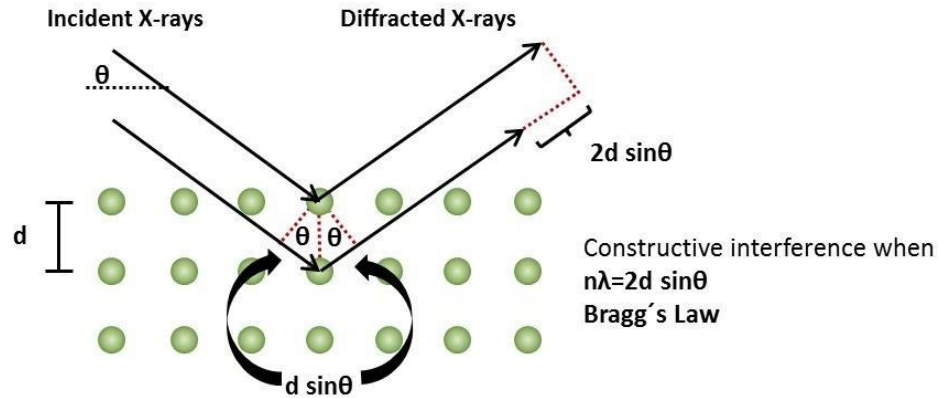
Figure 13 phenomenon when the x-rays interact with the sample.[47]

In XRD the corresponding X-ray beams having a wavelength extended from 0.7Å to 2 Å. whichincident on a sample and diffracts by a crystalline phase in the sample in accordance with Bragg'sLaw.

$$2dsin\theta = n\lambda$$

$$(3.1)$$

In the crystalline phase, the spacing between atomic planes is known as d. The wavelength of the X-ray is λ. The diffraction angle 2θ and sample inclination are used to measure the intensity of diffracted X-rays. The structural properties and crystalline phases are investigated by the diffraction pattern. XRD is a non-destructive technique, and sample preparation is not required.

3.2.1. **Structural Studies Using XRD**

We can observe many different features from XRD analysis.

- Crystallite size

- Lattice parameters

- Calculating X-ray density

- Calculating porosity

- The mass density

- Phase confirmation

Lattice Parameter

The unit cell of a crystal is defined by the lattice constant. It is the length of one of the cell's edges or an angle formed between the edges. It is also known as the lattice constant or the lattice parameter. The lattice constant is the constant distance between the lattice points. The lattice constant is calculated using the equation below.

$$a = \frac{\lambda(h^2+k^2+l^2)^{1/2}}{2sin\theta} \qquad (3.2)$$

In the above equation, lattice constant is "a", the wavelength of X-ray radiation is 1.54 for Cukα, miller indices are "h, k, l" and diffraction angle is θ.

Crystallite Size

The particle size has a significant impact on the structural characteristics. It is compared to JCPDS cards for the identification and validation of the experimentally acquired diffraction pattern. The Debye-Sherrer equation, which is used to determine particle size, states that peak width is inversely proportional to crystal size. Therefore, peak broadening in XRD analysis is proportional to the small crystallite size. To determine particle size, utilize the Debye-Sherrer equation.

$$D = \frac{0.9\lambda}{\beta cos\theta} \qquad (3.3)$$

λ represents the incident X-ray wavelength and θ and β represent diffraction angle and full width half maximum respectively.

3.2.2. Advantages of XRD:
- Non-destructive technique.

- No sample preparation is required.

- Computer-assisted material determination

- Fast determination of defects, stresses, strains, crystallite sizes, and orientation of singlecrystal of sample.
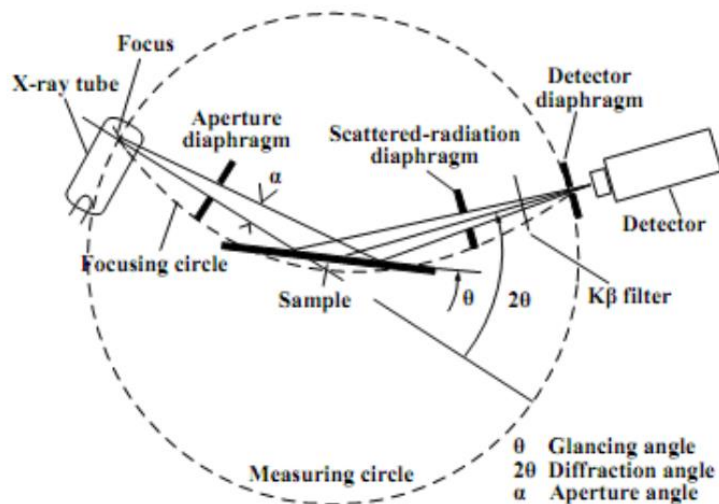
Figure 14 Schematic diagram of XRD [48]

3.3. FTIR (Fourier Transform Infra-Red Spectroscopy):

FTIR is a method for obtaining an infrared spectrum of a solid, liquid, or gas absorption or emission. High spectral resolution data throughout a broad-spectrum range are concurrently collected by an FTIR spectrometer. In comparison to a dispersive spectrometer, which measures intensity over a broad wavelength range at a time, this offers a substantial advantage.
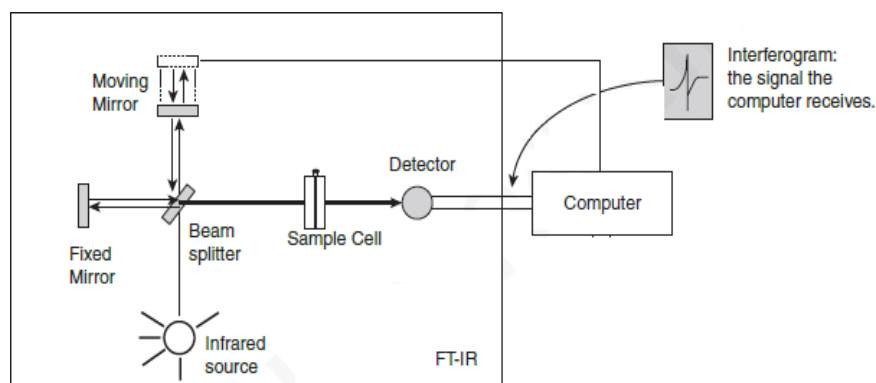
Figure 15 Schematic diagram of FTIR[49].

FTIR is an analytical method for examining chemical groups in the sample. The infrared electromagnetic radiation that strikes the sample ranges in wavelength from 10,000 cm^{-1} to 100 cm^{-1} and from 4,000 cm^{-1} to 400 cm^{-1}. Infrared radiation is emitted from the sample, and when it is absorbed by a molecule, it causes the molecule to vibrate. Then, using spectroscopy, these vibrations are investigated.

3.3.1. Working Principle of FTIR

The fundamental component of FTIR spectrometers, the Michelson interferometer, is used to splitone light beam into two such that the trajectories of the two rays are different. This is how FTIR operates. The two dispersed rays are then collected by the Michelson interferometer and sent to the detector, where the intensity difference between the two beams is determined as a function ofthe path difference.

3.3.2. The Components of the FTIR spectrometer

The basic components of the apparatus are a source, an interferometer, a sample chamber, a detector, an amplifier, an A/D converter, and a computer. Through an interferometer, the source's radiation passes the sample and moves toward the detector. For signal amplification and conversion to a digital signal, an amplifier, and analog-to-digital converter are used. Finally, the signal containing the Fourier transform data is received by the computer. Fig.15 depicts the FTIR spectrometer and it's function.

3.4. SEM (Scanning Electron Microscopy):

SEM is a technique used for the study of the morphology of the sample surface and its crystal structure. SEM creates images of a specimen by scanning its surface with the central beam of electrons. Electrons interact with the atoms of a specimen. And then it produces various signals that contain data about the surface topography and formation of the specimen. The position of the beam is collaborated with the intensity of the recognized signals to produce an image. Using an Everhart-Thornley detector, secondary electrons released by atoms excited by the electron beam are found in SEM. When the high energy beam contacts the sample surface, the following information is obtained.

- Composition of the sample.
- Phase mapping

- Topography of the sample.

SEM can attain a resolution improved by 1 nanometer. The magnification of SEM can be controlled from 10 to 500,000 times [50, 51].
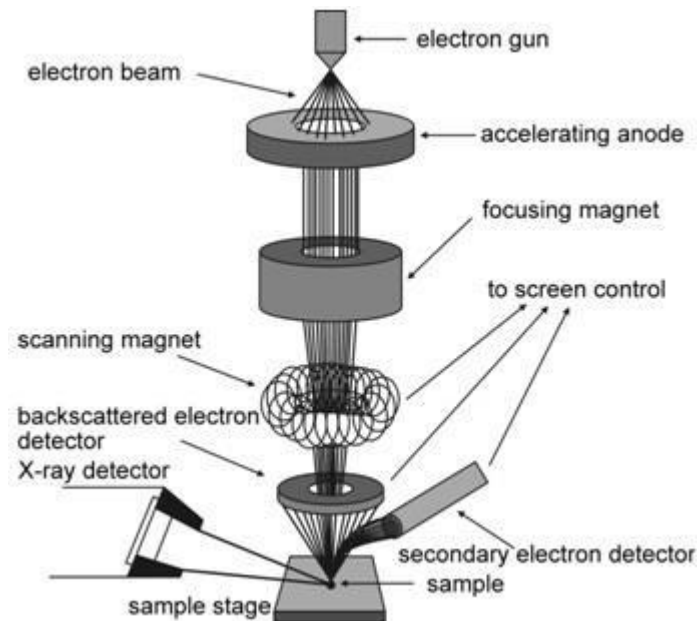
Figure 16 Schematic diagram of SEM [52]

3.4.1. Parts of SEM

The SEM's principal components are as follows:

- Electron gun
- Anode
- Electromagnetic lens
- Specimen stage
- Magnetic scanning coils
- Secondary electron detectors

3.4.2. Working Phenomena of SEM

Inside the SEM is an electron gun that aids in the bombardment of electrons. The incident electrons are directed onto the target via magnetic coils and a lens. The detectors catch the bouncing electrons and send them to the monitor, which creates the image as shown in Fig.16.

3.4.3. Interaction of Incident Electron beam with sample

An electron source, electromagnetic lenses, and electron detectors make up a scanning electron microscope (SEM). It uses an electron beam rather than light since it is based on the wave-particleduality theory. The lenses are used to accelerate, focus,

and expel the electron beam onto a sample. Primary electrons lose energy when they hit the sample surface because of collisions and absorption with certain interaction volumes in the sample. Secondary electrons (SE) and back scattered electrons are produced by this interaction (BSE). Back scattered electrons are the result of elastic scattering between the incident electron beam and the sample, whereas SE is the consequence of inelastic scattering caused by the atoms within the samples. Backscatteredelectrons come from deeper areas and southeast from the sample's surface.
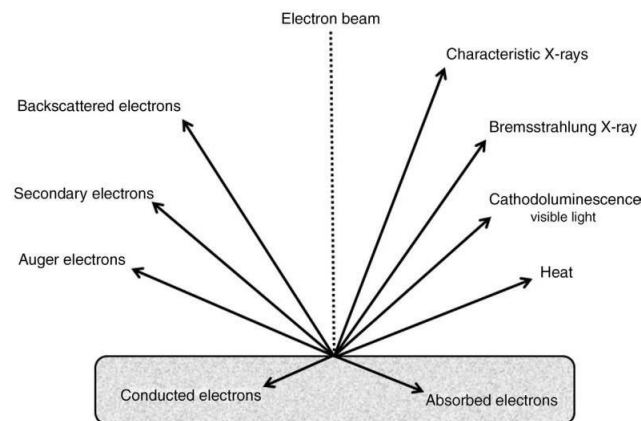
Figure 17 Interaction of electron beam with sample surface [53]

3.5. EDS (Energy dispersive spectroscopy)

The elemental makeup of the material is determined using the energy dispersion X-Ray (EDS) technique. EDS system works in tandem with a scanning electron microscope (SEM) and cannot function on its own without a SEM.

During the EDS Analysis, the sample in the specimen chamber SEM is blasted with an electron beam. When the bombarded electrons from the electron column hit with the material under observation, some of the electrons are knocked out. The internal shell electrons that are knocked out leave a void behind them, which is subsequently occupied by outer shell electrons. The electron gives off X-rays as it fills the gap from its outer shell to release its energy. The shell that an electron exits and subsequently moves to determines how much energy is released. Additionally, during the transfer process, each element's atom emits X-rays with a different energy level. Now, it can identify the atoms by gathering and measuring the total energy emitted by the sample in the form of X-rays. The peaks in the EDS spectrum correspond to different energy levels. Each peak in this spectrum only corresponds to an atom of a certain element. The length of the peak in the spectrum can be used to determine

the element concentration; the longer the peak, the more weight percent of the element is present in the sample.

3.6. VSM (Vibrating Sample Magnetometer)

The VSM is less sensitive to sample mass and size than an alternating gradient magnetometer up to a significant range. In this method, the sample is put into an external magnetic field that is steady and uniform and causes the sample to become magnetized. The external magnetic field is then perturbed as the magnetized sample is vibrated.

To quantify these alterations, the sample can be surrounded by a collection of coils or a few magnetic field sensors. In the case of coils, for instance, the magnetic flux piercing the coils will change, causing the coils to produce an emf (electro motive force). The emf produced in coils for a specific coil geometry depends on the magnetization of the sample, the external magnetic field, the amplitude and frequency of vibration. We can determine the value for magnetization from emf with the right manipulation.

A vibrating sample magnetometer measures the magnetic properties of different samples. Wecan measure saturation magnetization, coercivity, and remanence. The basic principle of vibrating sample magnetometer is Faraday law of induction. This shows that when the magnetic field is changed electric field is induced [54].
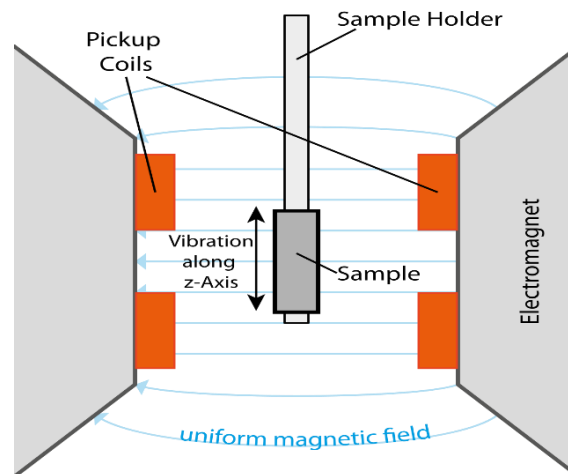
Figure 18 Schematics of Vibrating sample magnetometer [55]

3.7. Dielectric Properties

Since it can measure a material's inductance (L), capacitance (C), and resistance (R), the LCR meter earned its name. LCR meters can be used to measure a material's conductivity, tangential loss, dielectric constant, and other dielectric properties.

Model Th 6500B dielectric tests were made using a Wayne Kerr impedance analyzer in the 100 Hz to 5MHz frequency band. Depending on the frequency range of the LCR meter, these qualities can be examined at a variety of frequencies.

For ferrites, the dielectric characteristics are crucial. Particularly when the components are utilized to create memory devices. Due to the tiny sample sizes in the nanoscale region, the dielectric characteristics become very crucial. Ferrites are the good materials for dielectrics. These have a variety of uses, including microwave and radio frequency. To research the dielectric characteristics of ferrites at various frequency ranges, this is crucial. The approaches used to prepare the ferrites have significant influence on the dielectric characteristics. At room temperature, the dielectric constant is measured between 100 Hz and 5 MHz. To fully explain various hypotheses, accurate measurement of the dielectric constant is important [56].

The relation given as can be used to get the dielectric constant.

$$\varepsilon' = \frac{c \times d}{A \times \varepsilon_0} \quad\quad\quad (3.4)$$

Where (A) represents the pellet's area, (d) represents its thickness of the pellet, (C) represents its capacitance, and (ε_o) represents the permittivity of empty space [57]. The ac conductivity can be formulated as:

$$\sigma_{ac} = J/E \quad\quad\quad (3.5)$$

Figure 19 Impedance Analyzer for Dielectric Properties (TT lab, SCME, NUST)

Electric current density (J) and electric field density (E) are both present here. The ac conductivity can be stated as, using the replaced values:

$$\sigma_{ac} = J/E = \varepsilon j\omega \qquad (3.6)$$

ε is the complex function can be defined as,

$$\varepsilon = \varepsilon' - \varepsilon'' \qquad (3.7)$$

The dissipation or loss factor can be written as,

$$\tan\delta = \varepsilon'' \div \varepsilon' \qquad (3.8)$$

where the actual dielectric constant is ε' and its imaginary component is ε''.

Finally, the relationship to determine ac conductivity is as follows:

$$\sigma_{ac} = 2\pi f \tan\delta \varepsilon' \varepsilon_o \qquad (3.9)$$

Where f is the applied frequency.

Chapter # 4

Results and Discussion

4.1. X-ray Diffraction

The structural analysis of $CoFe_2O_4$ and $Ni_xZn_xCo_{1-2x}Fe_2O_4$ with varying concentrations 'x' was done by powder X-ray diffraction technique using CuKα radiation with CuKα = 1.5418 Å and scanning angle 2θ (20 to 80°).

4.1.1. X-ray Diffraction Analysis of Cobalt Ferrite (CoFe$_2$O$_4$)

XRD measurements done on $CoFe_2O_4$ nanoparticles sintered at 600 °C for 2 hours. Figure 20 shows the XRD findings that are consistent with the cubic spinel structure. The XRD data are also used to estimate the sample's particle size, lattice constant, and phase identification. The sample's single-phase formation, which revealed that the sample is polycrystalline in nature, supports the XRD results. The average crystalline size of ferrite nanocrystals is calculated by Debye Scherrer formula.

$$D = K\lambda \, / \, \text{ß}\cos\boldsymbol{\theta} \tag{4.1}$$

where K is 0.9, k is 1.54060 A$^\circ$, ß is full width at half maximum of the diffraction peak, and θ is the diffraction angle. According to the JCPDS card (22–1086), the final product is $CoFe_2O_4$ nanoparticles with the predicted closed-packed face-centered cubic arrangement structure, according to diffraction of the pure cobalt ferrite ($CoFe_2O_4$) powder calcined at 600°C for two hours. The crystallinity of the synthesized product is demonstrated by the conspicuous presence of peak (3 1 1) at 35.7^o, whilethe FWHM demonstrates the creation of a crystallite size. The absence of any additional peaks onthe pattern (apart from the cubic arrangement peak) indicates that the synthesized product was freeof impurities. The crystallite size was determined to be 28 nm using equation (4.1). The (311) plane's full-width half maximum is considered in Debye's formula for calculating the result.
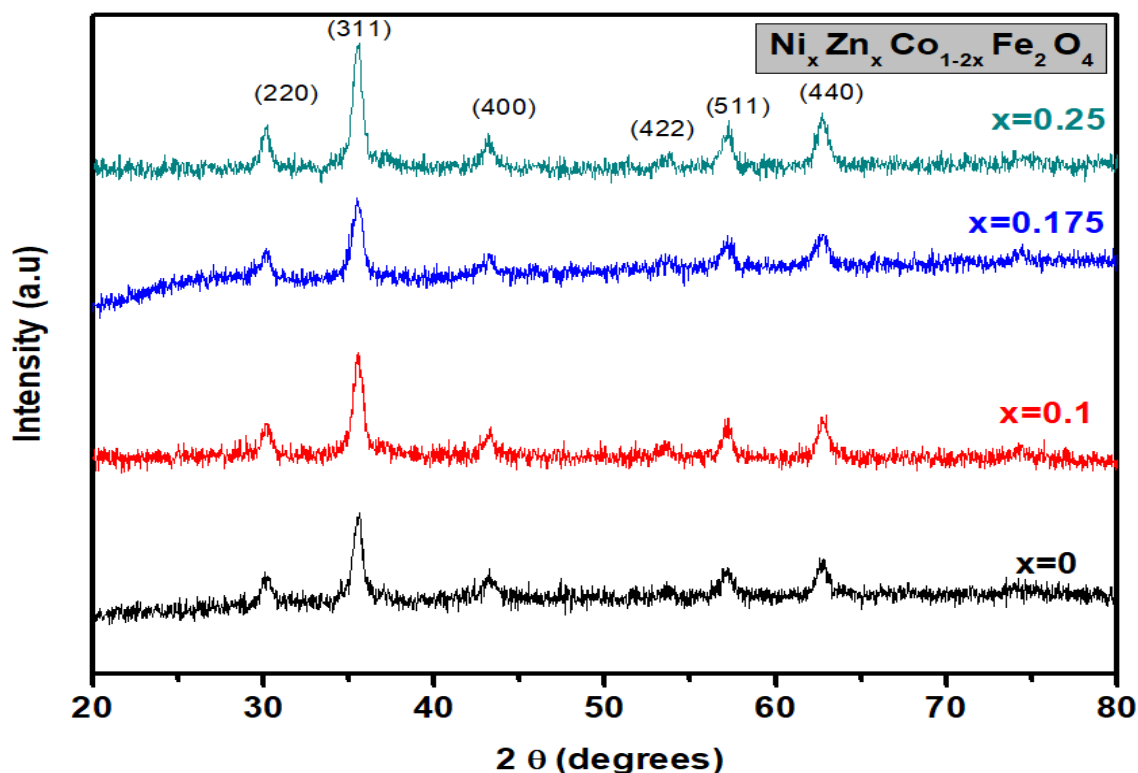
Figure 20 Graphical representation of XRD data for $Ni_xZn_xCo_{1-2x}Fe_2O_4$ (x= 0, 0.1, 0.175, 0.25) Nanoparticles

4.1.2. X-RAY Diffraction of $Ni_xZn_xCo_{1-2x}Fe_2O_4$

The Powder X-Ray Diffraction Technique was exercised to investigate the structure and phase formation of the prepared Nickel and Zinc doped Cobalt ferrite Powder with different concentrations. The X-Ray powder Diffraction of the Nickel Zinc doped Cobalt ferrite powder shown in (Fig.20), calcinated at $600\,^{\circ}$C for 2 hours showed that the final product is $Ni_x Zn_x Co_{1-2x} Fe_2O_4$ nanoparticles (x= 0.1, 0.175, 0.25). The peaks were indexed from JCPDS (Joint Committee on Powder Diffraction Standards) card # JCPDS-ICDD – 22–1086, JCPDS-ICDD 10-0325, JCPDS-ICDD 22-1012. The XRD pattern of Nickel and Zinc doped Cobalt ferrite confirmed the desired closed-packed face-centered cubic arrangement structure.

All the samples illustrate well-resolved diffraction peaks positioned at 2θ =30.1º, 35.7º,43.3º, 53.8º, 57.2º and 62.82º corresponding to their respective planes (2 2 0), (3 1 1), (4 0 0), (4 2 2), (5 1 1) and (4 4 0) which verify the formation of face-centered cubic spinel ferrite, the intensity of the peak (3 1 1) is increasing, showing an increase in crystallinity, owing to the formation of more and more defects with increasing concentration of nickel and zinc. The mean crystallite size 'D' and lattice parameter

42

'a' for each XRD Pattern was calculated, for the most intense peak (3 1 1) using the equation (4.1) shown in table 4.1.

Table.4.1. The Average crystallite size and lattice parameter calculated from the XRD patterns.

X=	Average Crystallite size (nm)	Lattice parameter 'a' at (3 1 1) (Å)
0	13.66	8.374
0.1	10.51	8.379
0.175	13.39	8.384
0.25	14.14	8.387

4.2. Scanning Electron Microscopy (SEM)

The prepared $CoFe_2O_4$ and $Ni_xZn_xCo_{1-2x}Fe_2O_4$ (x= 0.1, 0.175, 0.25) nanoparticles using the coprecipitation method, were analyzed by Low vacuum scanning electron microscope (JSM6490A), operating at 20 kV with a magnification range of 100 X – 70000 X, With the use of ultrasonication, the samples were dissolved in deionized water, and when uniform dispersions were obtained, then dispersion droplets were applied on a glass slide and allowed to dry. The specimens were made conductive by applying a gold coating of a few nanometers with the aid of a sputter coater (JFC1500). So pure $CoFe_2O_4$ and $Ni_x Zn_xCo_{1-2x}Fe_2O_4$ (x= 0.1, 0.175, 0.25) and their loading data are presented below.

Images of $CoFe_2O_4$ and $Ni_xZn_xCo_{1-2x}Fe_2O_4$ (x= 0.1, 0.175, 0.25) that were synthesized by co-precipitation at 600° C are depicted in Fig. 21 (a-d), respectively. Clustering is observed in samples. According to images, as the concentration of nickel and zinc increases, the nanoparticles of $Ni_xZn_xCo_{1-2x}Fe_2O_4$ become more magnetic and hence form clusters. The obtained average particle size by 'image j viewer' software was 26.3 nm.
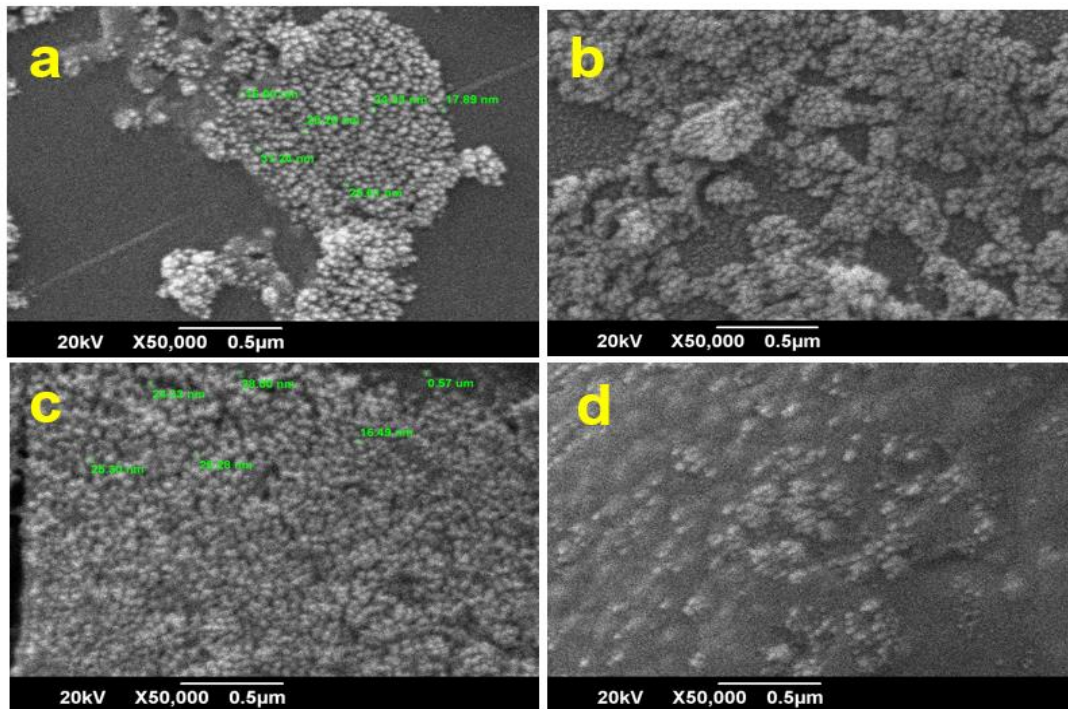
Figure 21 (a-d) SEM image of $Ni_xZn_xCo_{1-2x}Fe_2O_4$ (x= 0, 0.1, 0.175,0.25) nanoparticle

Fig.21(a-d) shows the surface morphologies of the $Ni_xZn_xCo_{1-2x}Fe_2O_4$ nanoparticle that were sintered. The SEM images demonstrate that all of the samples exhibit a compact arrangement of homogenous nanoparticles that are agglomerated and have a diameter that ranges from 12 to 34 nm. The particles are spherical and have a compact arrangement. Increases in nickel and zinc content result in a decrease in the total surface-free energy [58, 59]. Nanoparticles aggregate because of the magnetic forces that exist between the particles. The morphologies do not significantly change as nickel and zinc content rises. The grain boundary energy has decreased as a result of sintering, creating a thick structure [60].

4.3. Energy Dispersive Spectroscopy EDS

EDX can be used to determine the atomic concentrations of various compositions. Energy dispersive x-rays were used to verify the elemental compositions of the produced samples. Fig.22(a) depicts the EDX spectrum at x=0.0 and confirms that cobalt, iron, and oxygen are present, and both atomic and weight percentages are displayed. The spectrum for x=0.1, 0.175, 0.25 is shown in Fig.22(b, c, d), except that nickel and zinc are used in place of cobalt and all other elements are the same as in the specimen for x=0.0. Possible causes of the extra low-intensity peaks include

contaminants in the raw material.
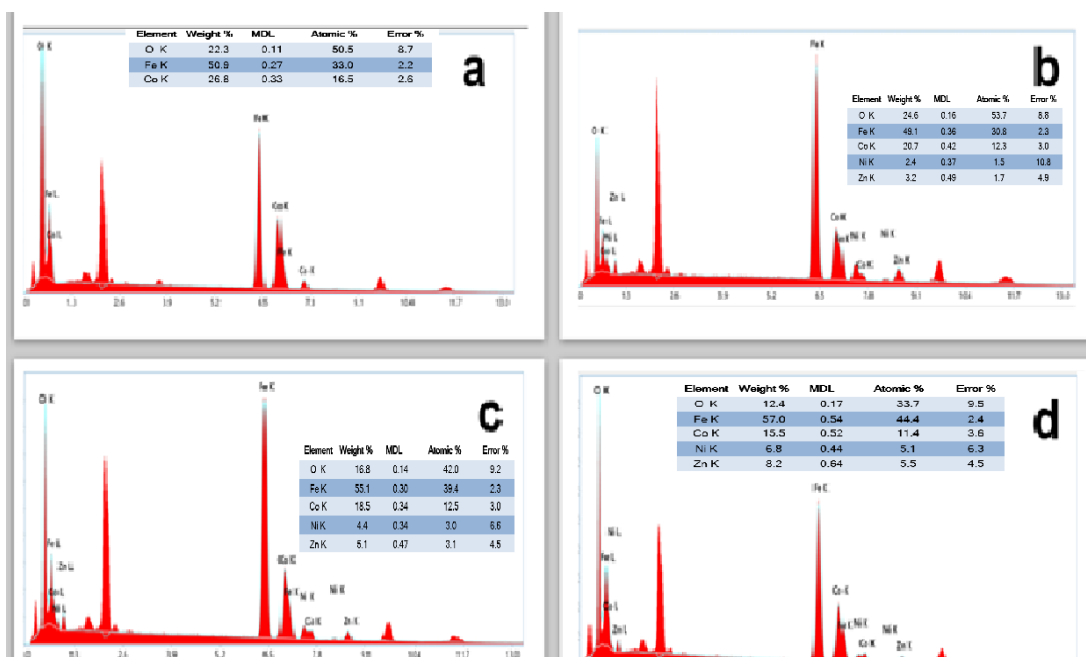
Figure 22 (a-d) Energy dispersive x-ray spectroscopy showing the elements present in all samples.

4.4. Fourier Transform Infrared Spectroscopy (FTIR)

The FTIR analysis of samples were carried out using the (Perkin Elmer-spectrum 100). As samples, KBr pallets were employed. The infrared radiation of a certain wavelength was used to illuminate the samples i.e. (350-4000 cm^{-1}).

4.4.1 Fourier transform infrared spectroscopy (FTIR) of $Ni_xZn_xCo_{1-2x}Fe_2O_4$

An important technique to assess the success of a solid-state reaction and look at spinel structural deformation brought on by foreign ions or cationic dispersion is infrared spectroscopy (IR) [61]. According to the FT-IR research, a tetrahedral cluster's normal vibrational mode is stronger than an octahedral cluster's. The octahedral group's larger bond length is the cause, whereas the tetrahedral cluster is shorter. The metal cations were situated closest to the oxygen ions in two separate sublattices of ferrites, namely the tetrahedral (A-sites) and octahedral sites (B-sites), in accordance with the geometric structure of ferrites [62].
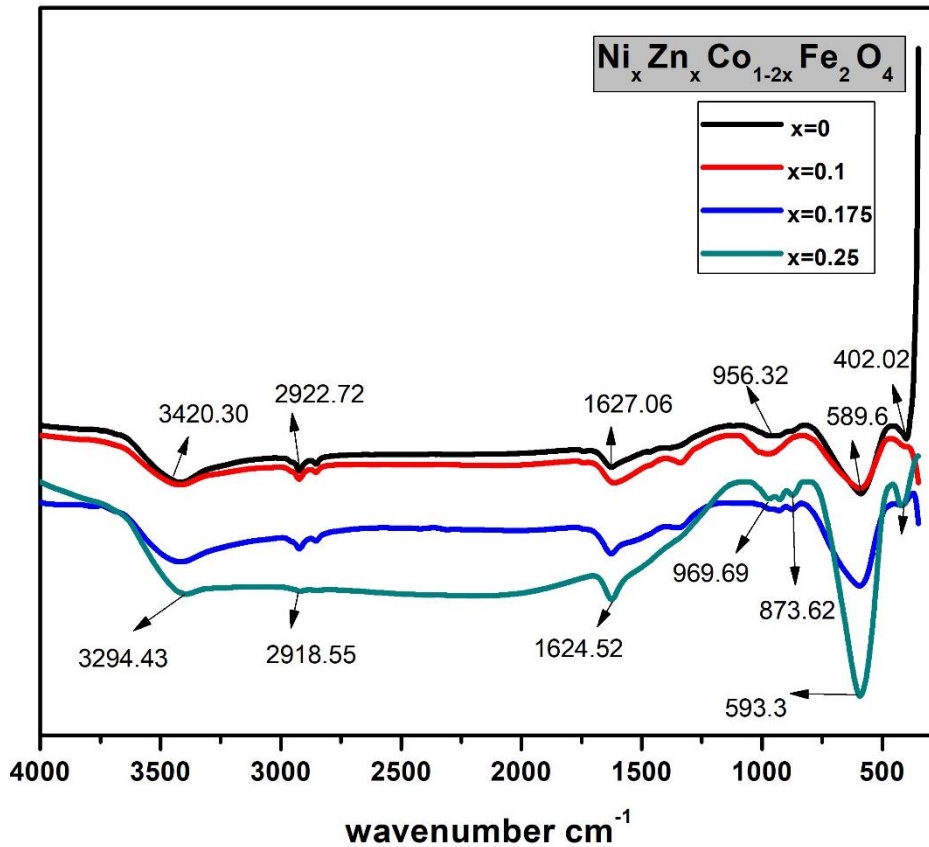
Figure 23 Plot of FTIR for $Ni_xZn_xCo_{1-2x}Fe_2O_4$ (x=0,0.1,0.175,0.25)

The FTIR spectra results of our sample show notable two frequency bands at 420 cm^{-1} and 594 cm^{-1} measured in the wavenumber range of 350 to 4000 cm^{-1} Showing a pure spinel phase. Due to the existence of tetrahedral complexes the frequency band is at a higher wavelength v_1 (589–595cm^{-1}) whereas the lower frequency band is v_2 (400 – 421cm^{-1}) due to the octahedral complexes [63] shown in Fig.24. The $Ni_xZn_xCo_{1-2x}Fe_2O_4$ ferrites' FT-IR spectra reveal two prominent absorption bands at 595-589cm^{-1} and 421 – 400 cm^{-1}. The vibrations of the metal-oxygen ion complexes in the tetrahedral and octahedral locations led to the assignment of these bands (v_1 and v_2). The Fe^{3+}- O_2 distance for tetrahedral and octahedral complexes differs, which causes the band position discrepancies (v_1 and v_2) to appear [64]. In general, the cation mass, bonding force, and cation-oxygen distance all affect the vibrational frequency [65].

The **table 4.2** listed the tetrahedral and octahedral metal complexes that correlate to the vibrationalfrequencies of $Ni_xZn_xCo_{1-2x}Fe_2O_4$ ferrites v_1 and v_2, respectively.

X	0	0.1	0.175	0.25
Tetrahedral band (v_1)	589.66 cm^{-1}	592.64 cm^{-1}	595.06 cm^{-1}	593.30 cm^{-1}
Octahedral band (v_2)	400.02 cm^{-1}	411.13 cm^{-1}	414 cm^{-1}	421.01cm^{-1}

4.5. Measurement of dielectric properties

The dielectric characteristics of $Ni_xZn_xCo_{1-2x}Fe_2O_4$ nanoparticles were tested using an RF Impedance/Material Analyzer in the 100 Hz – 5 MHz frequency range. We discovered the dielectric constant, dielectric loss (actual permittivity), tangent loss (imaginary permittivity), and ac conductivity in relation to frequency from an RF Impedance/Material Analyzer. Theoretically, it is assumed that as frequency rises, the dielectric constant falls. As the dielectric constant results from material polarization, polarization in ferrites is caused by an electron transfer between the Fe^{2+} and Fe^{3+} sites. After a certain frequency limit, this exchange of electrons ceases and does not follow the alternating field, so the dielectric remains constant. As the frequency rises, the interchange of electrons between Fe^{2+} and Fe^{3+} ions decrease.

4.5.1. Dielectric Properties of $Ni_xZn_xCo_{1-2x}Fe_2O_4$

The RF Impedance/Material analyzer measured the dielectric constant as 441.98 in the instance of a sample of $Ni_xZn_xCo_{1-2x}Fe_2O_4$ for x=0 at a frequency of 100 Hz, and it decreased with increasing frequency in accordance with theoretical predictions before becoming constant after a certain frequency. As can be shown in Fig.25, the dielectric constant of $Ni_xZn_xCo_{1-2x}$ Fe_2O_4 nanoparticles increases as the value of 'x' increases. The rate of electron exchange between Fe^{2+} and Fe^{3+} rises due to an increase in the value of 'x', which in turn enhances polarization. For $Ni_xZn_xCo_{1-2x}Fe_2O_4$ nanoparticles made with different concentrations of 'x' (0.1, 0.175, 0.25) the dielectric constant measured at 100 Hz is 504.6, 570.1, 2358.2.
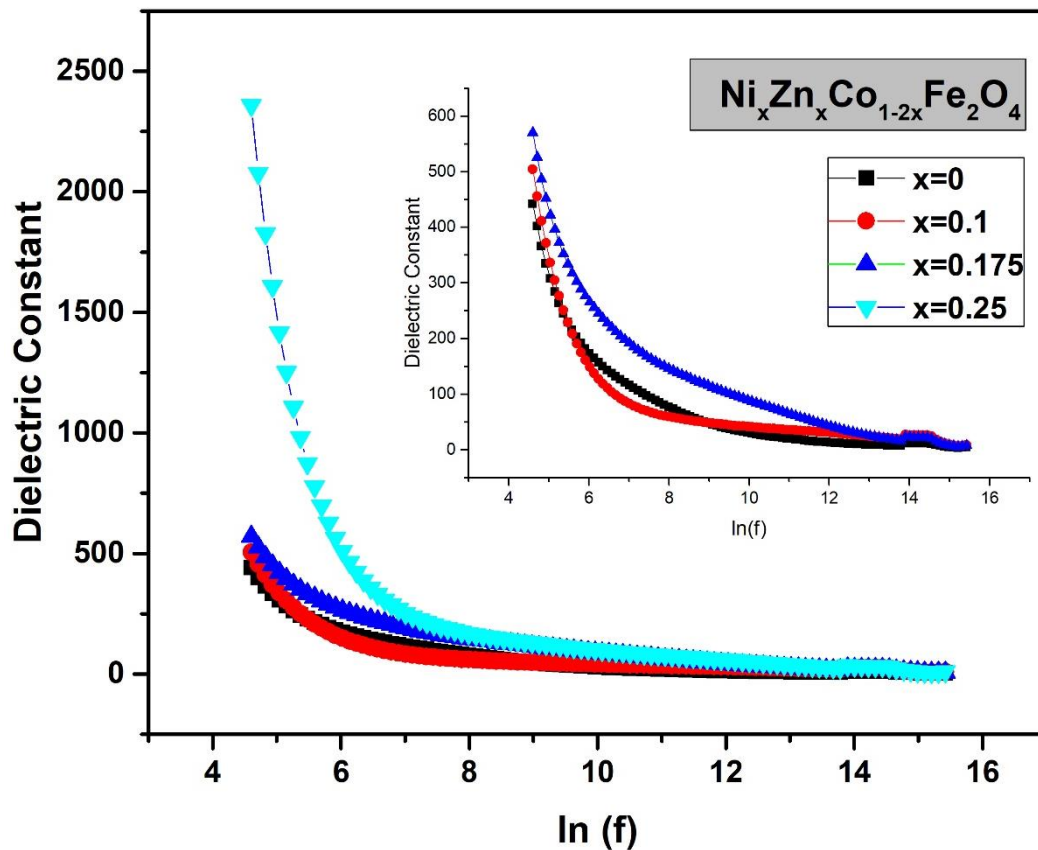
Figure 24 Graph of dielectric constant vs ln(f) of $Ni_xZn_xCo_{1-2x}Fe_2O_4$ nanoparticles

The graph of frequency vs dielectric loss is shown in Fig.25. The permittivity of the imaginary component theoretically decreases as frequency increases and remains unchanged after a certain frequency. Similar results were obtained from our samples, as shown in Fig.25. The imaginary permittivity of a $CoFe_2O_4$ sample is 617.6 at 100 Hz, although it continues to fall with higher frequencies before becoming constant. When in the case of $CoFe_2O_4$, the value of imaginary permittivity is equal to 617.6, and it is evident from the graph that this value rises as the concentration of Nickel and Zinc in $Ni_xZn_xCo_{1-2x}Fe_2O_4$ nanoparticles samples is increased. For (x = 0.1, 0.175,0.25) $Ni_xZn_xCo_{1-2x}Fe_2O_4$ nanoparticles, the values for imaginary permittivity are 848.01, 605.2, and 5881.7, respectively [66].

The ratio of the dielectric loss factor to the dielectric constant, which is plotted as the dielectric losstangent Vs frequency in Fig.26, is displayed with rising frequency for the corresponding Nickel and Zinc concentrations as follows. It behaved in a manner that was comparable to both dielectric loss and dielectric constant [67].

The dielectric materials are composed of several well-conducted grains separated by narrow, poorly conducting-grain boundaries. The charge carriers from the grain will

easily travel when the external electric field is introduced and gathered at the grain boundaries. This process will produce significantpolarization and a high dielectric constant. The electrical energy needed to rotate dipolar molecules isoften absorbed by the dielectric material, causing dielectric losses to occur [68].
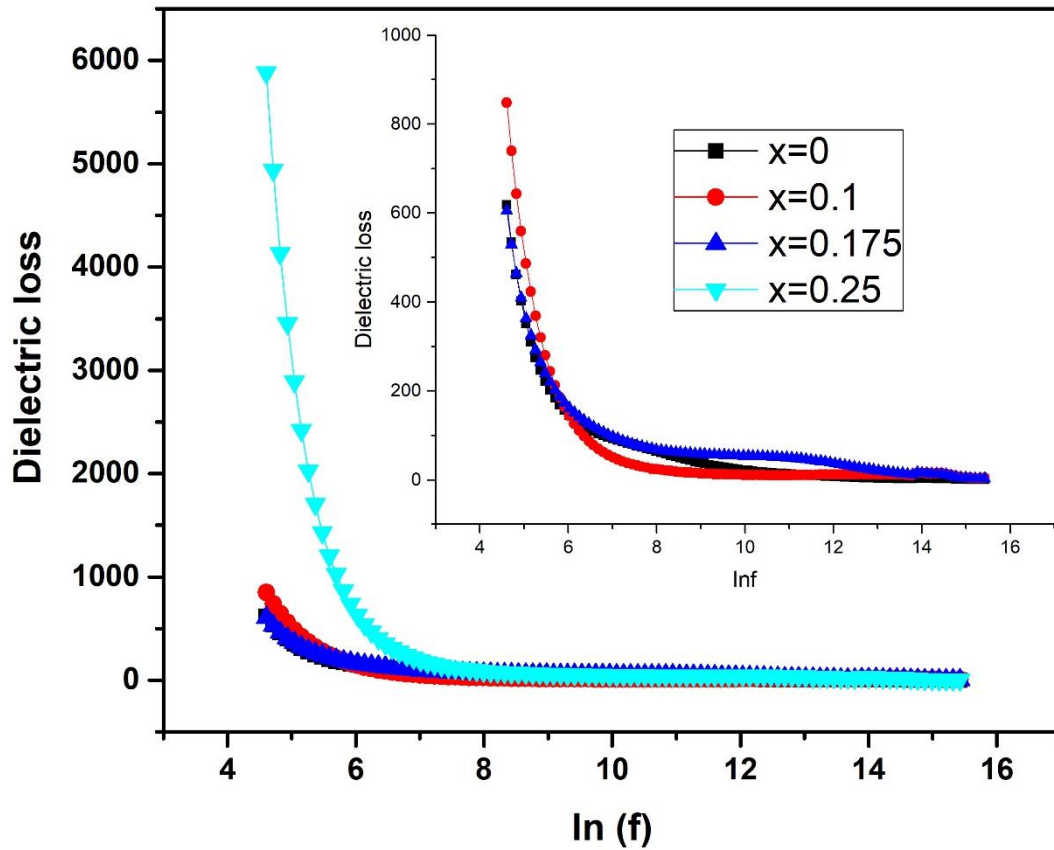
Figure 25 Dielectric loss graph vs ln (f) for Ni x Zn x Co $_{1-2x}$ Fe2O4 (x=0,0.1,0.175,0.25) nanoparticles
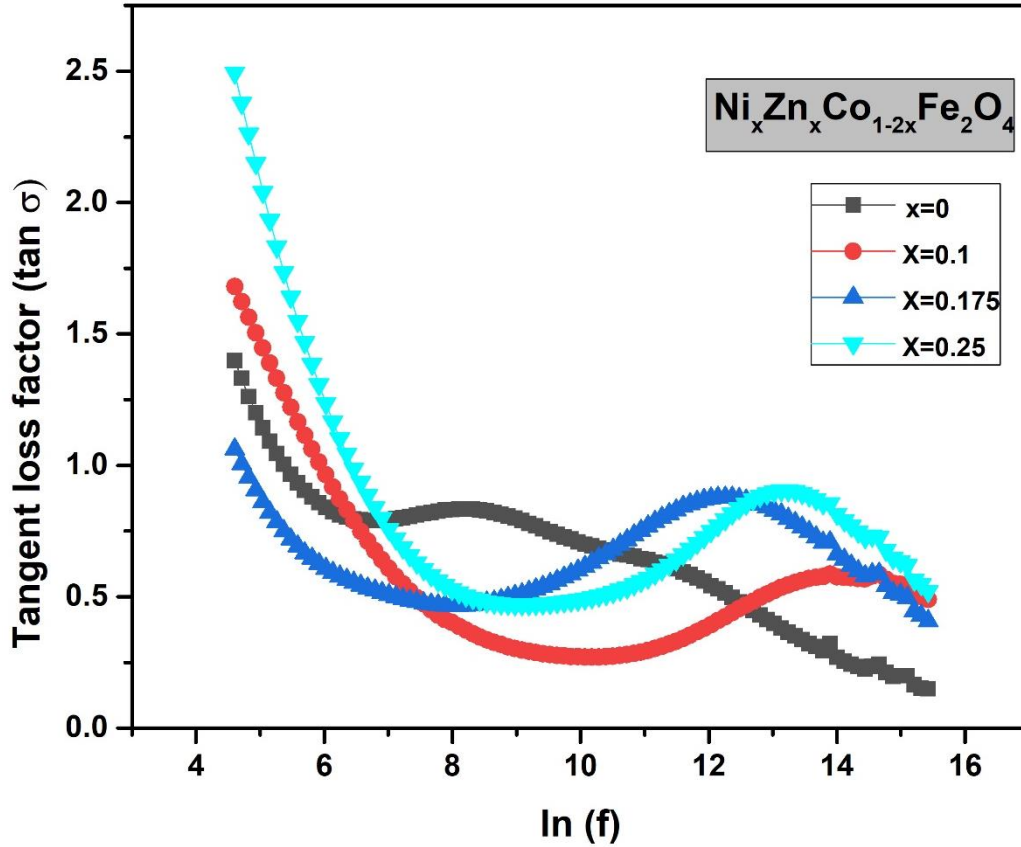
Figure 26 Tangent loss vs ln (f) graph of $Ni_xZn_xCo_{1-2x}Fe_2O_4$ (x=0,0.1,0.175,0.25)

we can see that samples made via chemical co-precipitation have a tiny peak in tan δ, which is shown in Fig.26.

The theory asserts that peaks are seen at resonance frequencies, or $\omega\tau = 1$, between the hopping charges in two valence states and the applied frequency, and τ denotes the relaxation period, which is inversely proportional to the jumping probability. With an increase in Ni^{2+} and Zn^{2+}, the peak shifts to a lower frequency. This can be attributed to high DC resistivity as a result of Ni^{2+} and Zn^{2+} replacing Fe^{2+} at B-sites, which are responsible for polarization in ferrites [68].

The dielectric tangential loss likewise exhibits a rising trend with increasing doping levels. Between ln 4 and ln 9, it exhibits greater values at low frequencies up to 550 Hz (Fig. 26). This is because electron hopping between Fe^{3+} and Fe^{2+} is greater at low frequencies of ln 4 to ln 9 but decreases at higher frequencies of ln 9 to ln 15, leading to a drop in dielectric tangent loss values.

When Cobalt ferrite is doped with x=0.25 Ni and Zn, the tangent loss value is enhanced to 2.49 from 1.39 at 100 Hz. Due to the increased number of charge carriers in doped samples, which necessitate a large amount of applied field energy for space

charge polarization, the dielectric tangent loss increased with concentration. Consequently, the dielectric tangent loss rose [69].

A rise in value with increasing Nickel content indicates an increase in hopping or jumping probability per unit time. The transfer of the relaxation peak to the higher frequency side is caused by an increase in nickel content because nickel likes the B-site, which enhances the dipole-dipole interaction and impedes dipole rotation [70].

4.6. AC Conductivity

The hopping model can be used to explain ac conductivity in ferrites. For low frequency ranges of 550Hz between ln 4 and ln 10, the ac conductivity is frequency independent, and an increasing trend maybe observed with increasing frequency throughout the range of 1 MHz between ln 10 and ln 14. (Fig.27). This behavior conforms to the Maxwell-Wagner type [71]. In accordance with this, the conductivity values between ln 4.5 and ln 10 are low at lower frequencies due to a considerable barrier at grain boundaries (related to dc conductivity) to the flow of electrons. Because of the more efficient hopping of electrons between Fe^{2+} and Fe^{3+} ions, grain boundary conductivity increases as frequency increases. Due to the gap between the radii of Co, Ni and Zn, grain boundaries contribute significantly.

It is obvious that the relationship between σ_{AC} and applied frequency is straightforward. With an increase in the applied angular frequency, σ_{AC} rises. It was discovered that the Zn-Ni spinel ferrites σ_{AC} rise when the applied frequency rises farther. This could be explained by the electron hoppingor exchange, such as $Fe^{3+} + e^{-} \Leftrightarrow Fe^{2+}$ or $Ni^{2+} + h^{+} \Leftrightarrow Ni^{3+}$, which happens when an electron transforms between two nearby Octahedral sites in the spinel lattice [72]. However, the Verwey process is used to explain why σ_{AC} is enhanced for the Zn spinel ferrite [72].

In other words, electron hopping between ions of the same element that are present in more than one valence state and are dispersed at random over crystallographically inequivalent lattice locations is possible. The number of alike ions perhaps manufactured while the processing of ferrite samples [73].
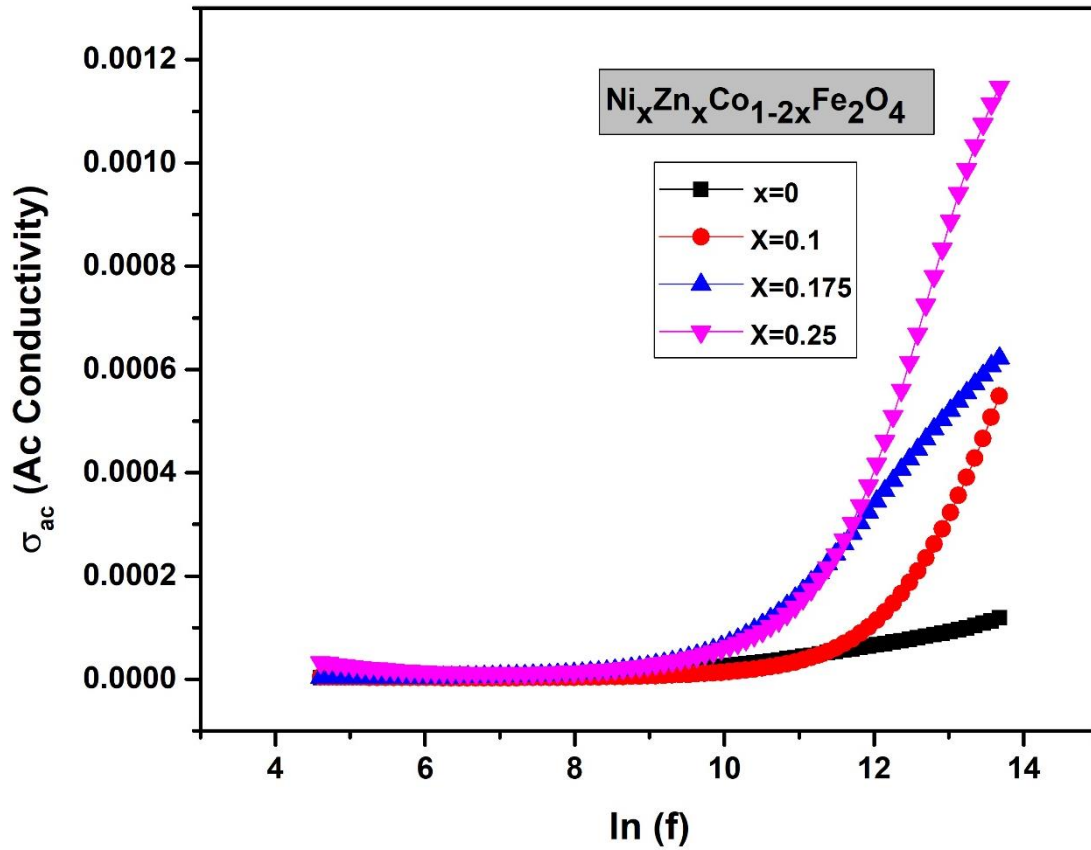
Figure 27 AC conductivity graph of $Ni_xZn_xCo_{1-2x}Fe_2O_4$ (x=0,0.1,0.175,0.25)

4.7. Impedance of $Ni_xZn_xCo_{1-2x}Fe_2O_4$

The real and imaginary components of impedance are illustrated in the figures below. The following relation makes it possible to see the impedance loss.

Real part of $Z´ = |Z| \cos(\theta)$

Imaginary part of $Z´´ = |Z| \sin(\theta)$

Where ''θ'' is phase angle which is given as $\theta = tan^{-1}(\frac{X}{R})$

R is the obtained resistance, while X is the reactance. where Z'' is the impedance loss, which equates to the material's series resistance. The total resistance of the circuit is displayed in the real component of impedance and is inversely related to the frequency of the applied AC voltage.

The impedance followed a similar trend to other electrical parameters, increasing at lower frequencies and then reducing as frequency increased before becoming constant. The movement of electrons between the Fe^{2+} and Fe^{3+} ions in ferrites also

affects impedance.

As shown in Fig.28, the graph's curve is steeper at lower frequencies and saturated at higher frequencies in the ferrite. The hopping of electrons is what causes this conduction mechanism[74].

The imaginary portion of impedance displays the ferrite's conduction; it can be seen that conduction linearly decreases with frequency at lower frequencies and becomes saturated at higher frequencies, as illustrated in Fig.29. Additionally, it has been found that incorporation of Ni^{2+} and Zn^{2+} first reduces and then increases the imaginary component of impedance. The graph's curves demonstrate that the grain boundaries have a significant impact; as a result, the impact of individual grains is minimal [75, 76].

Plotted in Fig.29, the complex impedance loss of the ferrite samples reveals that the complex impedance loss (Z'') is reached at higher frequencies as a result of a significant contribution from   the grains and grain boundary resistances [77]. Although conductivity would be ignored at grain borders, the observed peak reflects the behavior of grain boundary resistivity dominating over it [75, 78].

Mixed spinel ferrites are valued for their strong magnetic and resistive characteristics, which make them suitable for EMI suppression and shielding applications. In certain situations, a completely resistive circuit with a net impedance of zero can aid in suppressing high-frequency noise and lowering EMI [79].
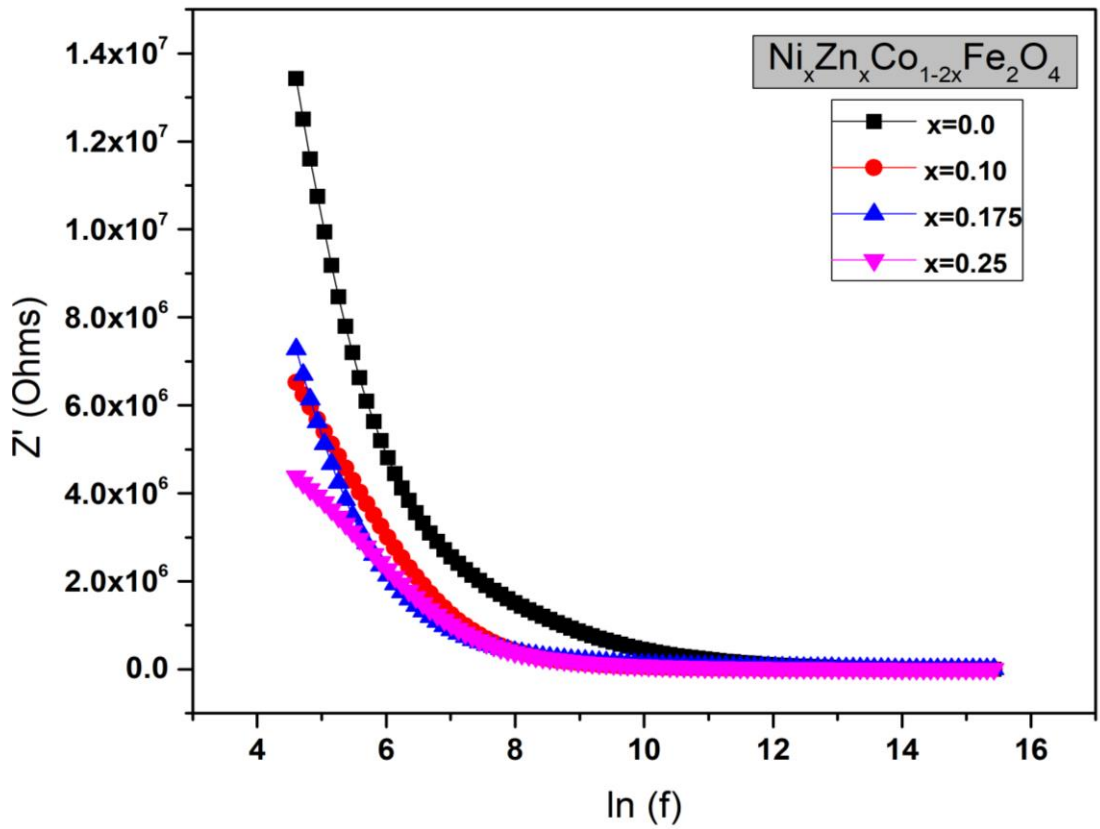
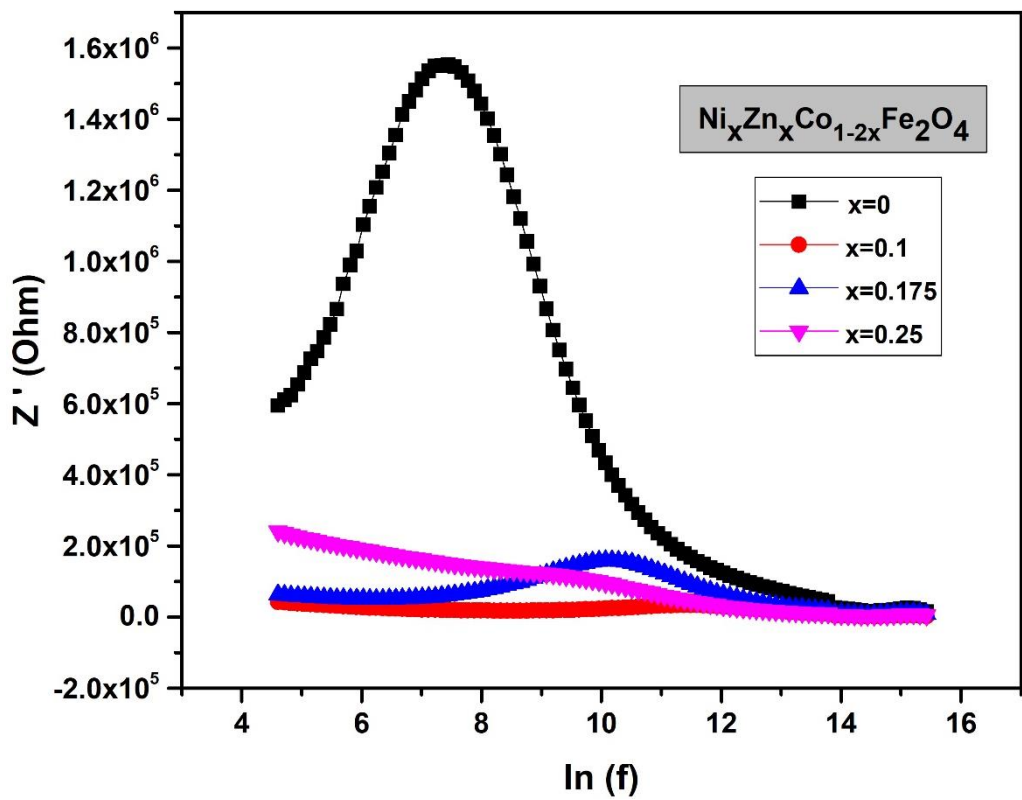*Figure 28 Impedance vs ln(f) graph of $Ni_xZn_xCo_{1-2x}Fe_2O_4$ (x=0,0.1,0.175,0.25)*

Figure 29 Imaginary part of impedance vs ln(f) of $Ni_xZn_xCo_{1-2x}Fe_2O_4$ (x=0,0.1,0.175,0.25)

4.8. Electric Modulus

Electric modulus is a very useful phenomenon that may be utilized to define the conduction and relaxation behavior of ionic and conducting ceramics. Complex electric modulus is sometimes known as the inverse of complex relative permittivity.

4.8.1. Electric Modulus of $Ni_xZn_xCo_{1-2x}Fe_2O_4$

Variation of the real and imaginary electric modulus portions with frequency is depicted in Fig.30 and 31, at constant temperature. Using complex modulus spectroscopy, the dielectric data measured over a wide frequency range at RT is further examined. In order to analyze the relaxation phenomena in electrically and ionically conducting materials and to identify the electrode polarizing effects that effectively annihilate, modulus spectroscopy is useful [80].

By the relation the complex dielectric and complex modulus is inversely proportional to eachother.

$$M = \varepsilon'/ (\varepsilon'^2 + \varepsilon''^2) \hspace{4cm} 4.2$$
$$M´ = \varepsilon''/ (\varepsilon'^2 + \varepsilon''^2) \hspace{4cm} 4.3$$

Electric modulus graphs are important for explaining the relaxation and conduction behavior of materials. Fig.30 and 31 depict the frequency dependent real and imaginary parts of the electric modulus at constant temperature for various nickel, zinc, and cobalt compositions. Above equations 4.2 and 4.3 were used to compute the real and imaginary parts of the electric modulus.

where M is the real part of the complex electric modulus and M´ is the imaginary part. Fig.31 depicts the fluctuation of the real component of the electric modulus with frequency for all compositions of Zn and Ni in cobalt ferrite.

Inferring the frequency dependence of the real (M) and imaginary (M′) components of electric modulus from the aforementioned equations is crucial for determining the material's relaxation mechanism. According to Fig.30, M exhibits the maximum value for x=0.00 and responds to higher frequencies quite effectively. The lower value of ε ′ at high frequencies is what it denotes. Its saturation is aided by the inadequacy of the restorative force and the release of space charge polarization close to the grain boundary. The electrical properties of the materials are guaranteed to be frequency independent by this phenomenon, which also happens at higher frequencies [66, 81, 82].

One must examine the variation of M′ as depicted in Fig.31 to provide an example

of the peakingbehavior (B). The peaking behavior is better illustrated using the hopping method since it more thoroughly shows how the charge carrier's transition. It is evident from the accompanying diagram that the charge carriers involved in the hopping process travel great distances while operating at low frequencies. The ability of charge carriers to travel short distances at higher frequencies, on the other hand, suggests that the polarization process has relaxed [83].
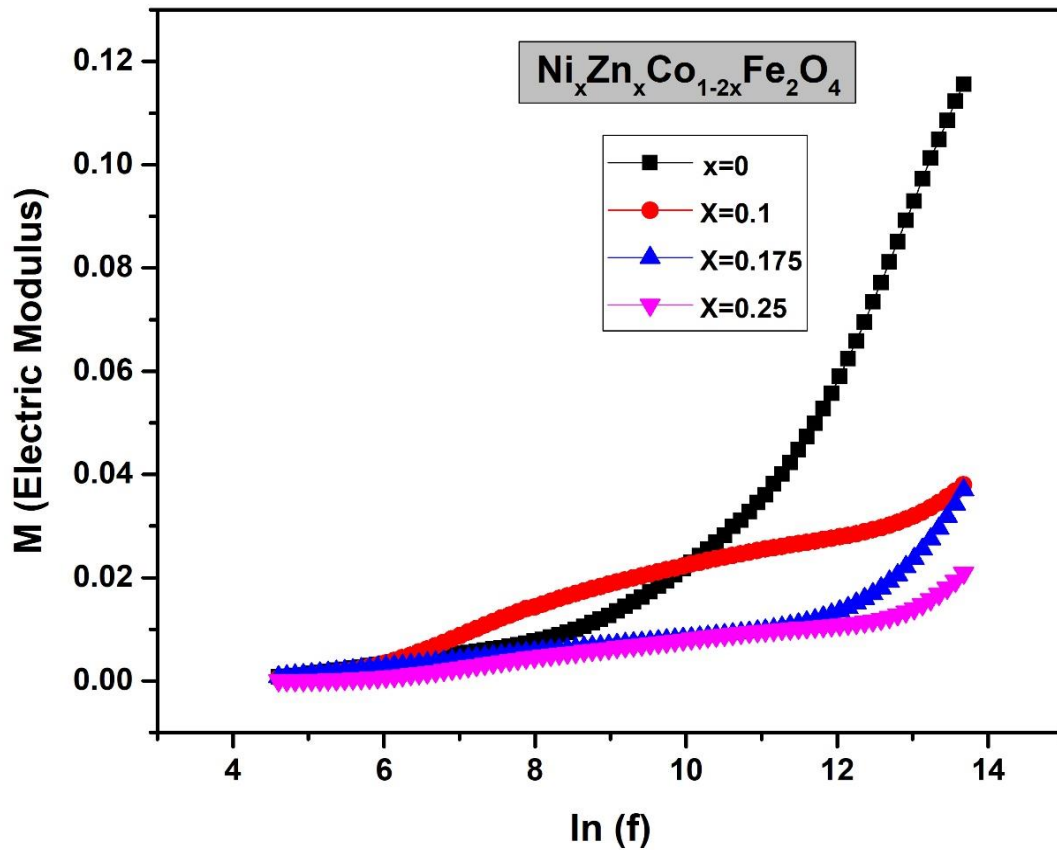
Figure 30 Electric modulus vs ln(f) of $Ni_xZn_xCo_{1-2x}$ Fe_2O_4 (x=0,0.1,0.175,0.25)
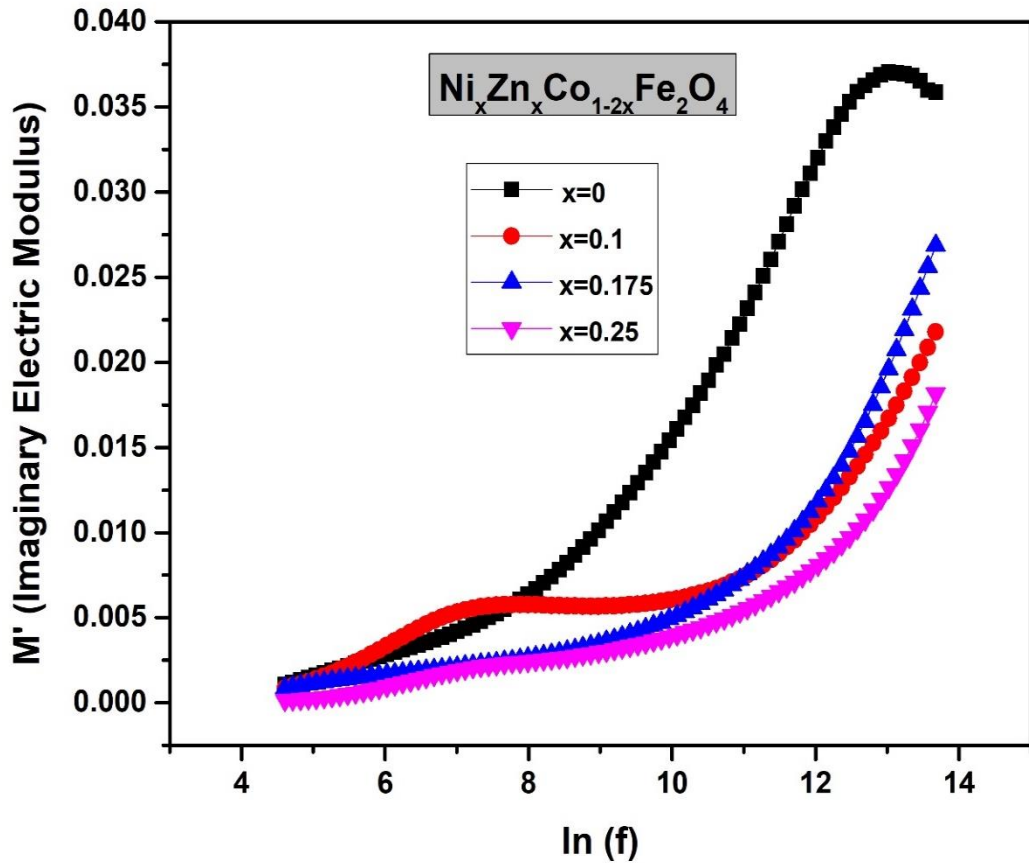
Figure 31 Imaginary part of Electric modulus vs ln(f) of $Ni_xZn_xCo_{1-2x}Fe_2O_4$
(x=0,0.1,0.175,0.25)

The Nyquist plot of the electric modulus (M′ vs M), shown in Fig.32, indicates when the material has relaxed this separation is assumed to be caused by the grain and grain border [83, 84]. The non-overlapping semicircular pattern in Fig.32 can be closely examined to reveal a distinct non- Debye type relaxation. At 600°C, nanoparticles exhibit two distinct, non-overlapping semicircular patterns [66, 82].
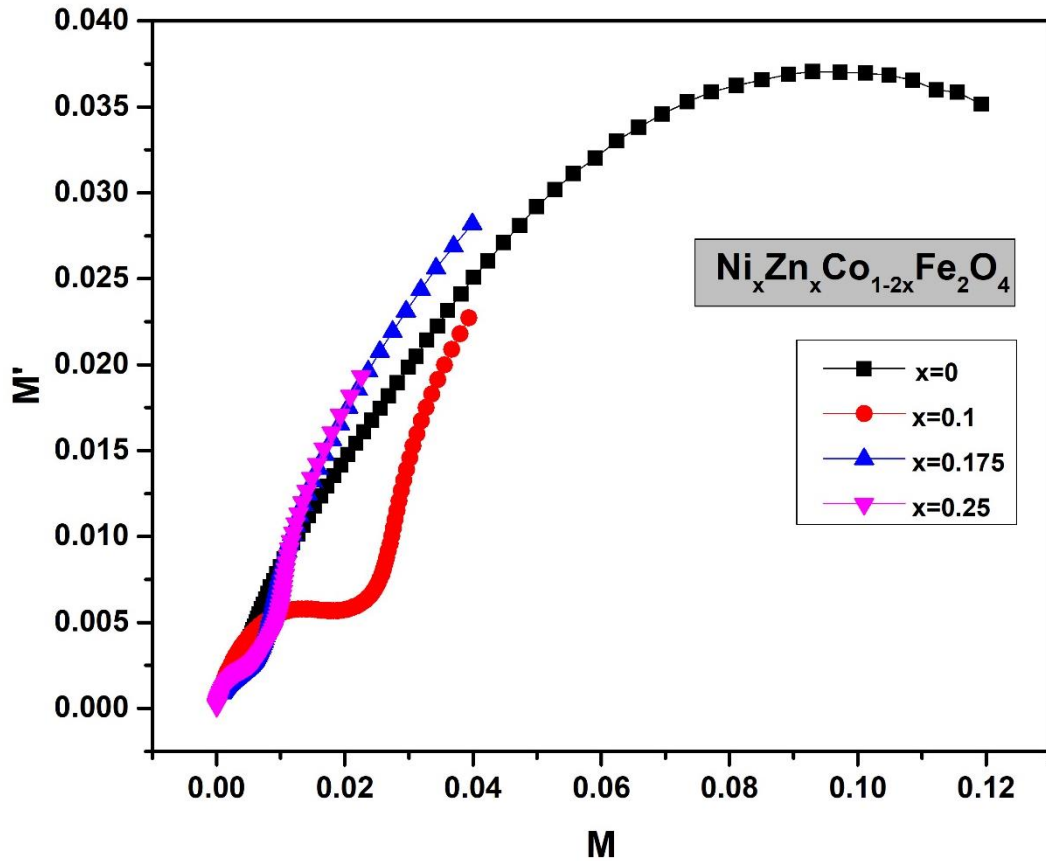
Figure 32 Cole-Cole plot of M' vs M of $Ni_xZn_xCo_{1-2x}Fe_2O_4$ (x= 0,0.1,0.175,0.25)

4.9. Magnetic Properties of $Ni_xZn_xCo_{1-2x}Fe_2O_4$

Using VSM, the magnetic characteristics of produced samples were investigated. Many factors, both intrinsic and extrinsic, have an impact on the magnetic properties of materials. The extrinsic factors are the synthesis process, microstructure, composition, and powder density while the intrinsic factors are the grain size, crystal defects, and lattice strain.

Magnetic parameters like saturation magnetization (M_S), coercivity (H_C), and remanence (M_r) were obtained from the M-H loop obtained from VSM at room temperature. The M_S value of $CoFe_2O_4$ is 64.02 emu/g. As the concentration of Ni and Zn increases the saturation magnetization value is increasing. But in x=0.25 concentration of Ni and Zn the saturation magnetization value drops to 59.44 emu/g. The reason behind this drop in M_S value is the increased concentration of zinc in the spinel ferrite. As the concentration is increased the grainboundaries increases hence the magnetic moment decreases.

Table.4.3. calculated values of saturation magnetization from hysteresisloop.

X	M_s (emu/g)
0	64.02
0.1	66.16
0.175	73.49
0.25	59.44

The ferromagnetic behavior of $CoFe_2O_4$ exhibits a significant hysteresis loop (Fig.33). While causing significant changes to the magnetic characteristics, doping with Zn and Ni ions also displays a ferromagnetic tendency; the hysteresis loop dramatically decreases with Zn and Ni concentration (Table 4.3). According to research, M_s rose with Zn and Ni to an ideal value of 73.49 emu/g at x=0.175 Zn and Ni concentration before falling to 59.44 emu/g at x=0.25 Zn and Ni content. Zn ions prefer to occupy the tetrahedral A sites of $CoFe_2O_4$ at lower concentrations, whereas, at larger concentrations, they have the propensity to shift to the octahedral B sites (Fe). It is quite intriguing that a magnetic Co ($\mu_B = 3$) can be replaced with a nonmagnetic Zn ($\mu_B = 0$), increasing the M_s value. With an increase in Zn content, it is discovered that H_C decreases. Although M_r reduces linearly and progressively with Zn concentration.

According to a paper [85] at a specific range of grain size, H_C and M_r become extremely sensitive to a change in grain size, which is compatible with the results that have been shown. For lower ranges of crystallite size (D), H_C and M_r showed a sharp decline as D increased, whereas a steady decline is shown as D gets higher. This is the significance of this relationship for the Zn-doped $CoFe_2O_4$ (Fig. 33) [86]. Also Due to nickel's lower magnetic moment, the magnetic characteristics show that as the Ni content rises, the Ms, Mr, Hc, decrease [36].
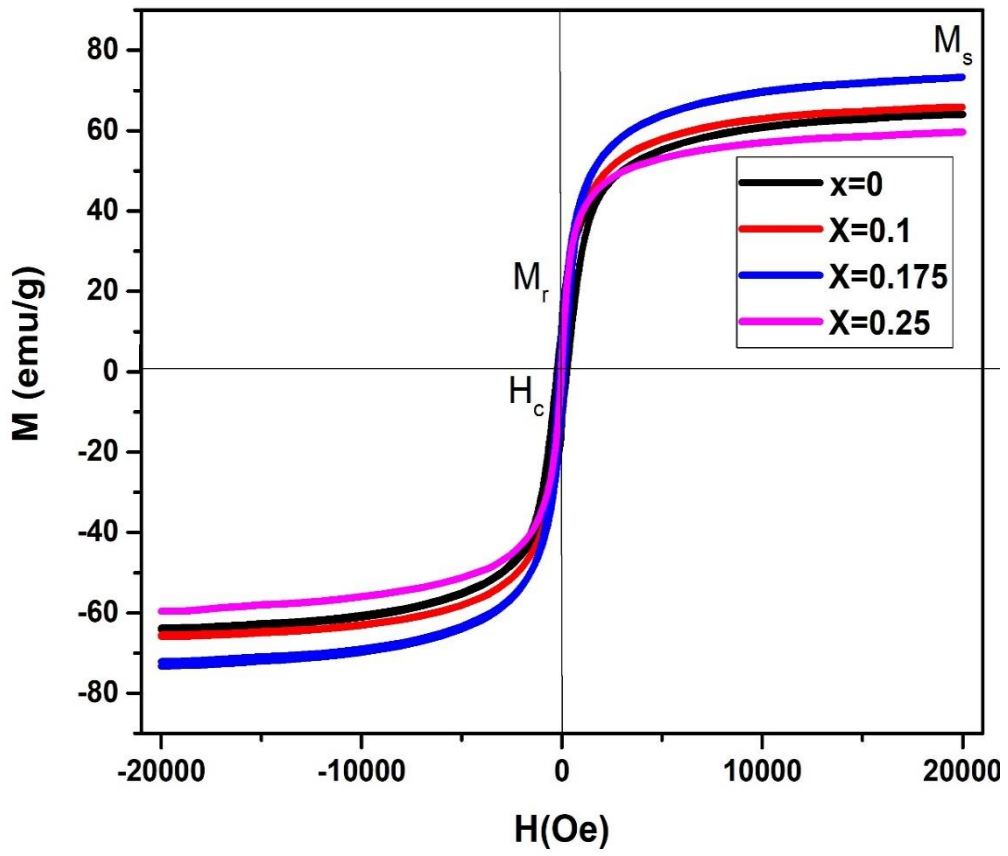
Figure 33 Hysteresis loop of $Ni_xZn_xCo_{1-2x}$ Fe_2O_4 (x=0,0.1,0.175,0.25)

Conclusion

In the present investigation, chemical co-precipitation was used to synthesize soft spinel ferrite $Ni_xZn_xCo_{1-2x}Fe_2O_4$ (x = 0, 0.1, 0.175, and 0.25). X-ray diffraction confirmed the single cubic phase in all four samples. When d- values acquired from XRD were compared with typical JCPDS cards using match software, the Cubic crystal structure of synthesized $Ni_xZn_xCo_{1-2x}Fe_2O_4$ was validated. The crystallite size was determined using Debye Scherrer's formula, ranging from 10 nm to 14 nm with a decreasing trend which agrees with the SEM results. SEM analysis also showed that the particles were in agglomerated form due to their magnetic nature. FT-IR analysis showed the shift in vibrational frequencies with increasing concentrations. Electrical properties have been investigated at frequency range of 100Hz to 5MHz. The increasing behavior of dielectric constant, dielectric loss, and tangent loss with rise in frequency has been observed. With an increase in Ni and Zn concentration, the dielectric constant was increased from 441.98 to 2538.2. At higher frequencies, the electronic polarization tends to dominate, causing an increase in the dielectric constant. Tangent loss factor was increased to 2.49414 from 1.3973 at 100 Hz, the frequency dependence of the tangent loss factor and dielectric constant in mixed spinel ferrites is an important characteristic that can be exploited in various applications, such as in electromagnetic interference shielding, microwave absorbers. conductivity was also increased at higher frequencies. The magnetic parameters of the synthesized samples, such as saturation magnetization and coercivity, were measured using a vibrating sample magnetometer. When x = 0.175, the saturation magnetization value increased from 64.023 emu/g to 73.49 emu/g, which is better than the value that have already been published [87]. In conclusion the $Ni_xZn_xCo_{1-2x}Fe_2O_4$ can be a promising candidate for Electromagnetic Interference Shielding in the low frequency region, according to the results of magnetodielectric analysis.

References

[1]   L. Filipponi, D. Sutherland, and I. N. Center, "Introduction to nanoscience and nanotechnologies," *NANOYOU Teachers Training Kit in Nanoscience and Nanotechnologies,* pp. 1-29, (2010).

[2]   K. E. Drexler, *Nanosystems: molecular machinery, manufacturing, and computation*: John Wiley & Sons, Inc., (1992).

[3]   G. BARIĆ, "Charles P. Poole Jr. i Frank J. Owens: Introduction to Nanotechnology," *Polimeri: časopis za plastiku i gumu,* vol. 24, pp. 134-135, (2003).

[4]   S. Feinberg, R. Williams, G. S. Hagler, J. Rickard, R. Brown, D. Garver*, et al.*, "Long-term evaluation of air sensor technology under ambient conditions in Denver, Colorado," *Atmospheric measurement techniques,* vol. 11, pp. 4605-4615, (2018).

[5]   C. A. Silvera Batista, R. G. Larson, and N. A. Kotov, "Nonadditivity of nanoparticle interactions," *Science,* vol. 350, p. 1242477, (2015).

[6]   L. Kiss, J. Söderlund, G. Niklasson, and C. Granqvist, "New approach to the origin of lognormal size distributions of nanoparticles," *Nanotechnology,* vol. 10, p. 25, (1999).

[7]   A. Aharoni, *Introduction to the Theory of Ferromagnetism* vol. 109: Clarendon Press, (2000).

[8]   A. Faraz, A. Maqsood, N. M. Ahmad, F. Ur-Rehman, and S. Ameer, "Mg0. 50Cu0. 5-xNixFe2O4 Spinel Nanoferrites: Structural, Electrical, Magnetic and YK angle Studies," in *Journal of Nano Research*, (2012), pp. 99-114.

[9]   A. Ghasemi, "The role of multi-walled carbon nanotubes on the magnetic and reflection loss characteristics of substituted strontium ferrite nanoparticles," *Journal of magnetism and magnetic materials,* vol. 330, pp. 163-168, (2013).

[10]   C. Tsay, K. Liu, T. Lin, and I. Lin, "Microwave sintering of NiCuZn ferrites and multilayer chip inductors," *Journal of Magnetism and Magnetic Materials,* vol. 209, pp. 189-192, (2000).

[11]   M. A. Pinheiro, L. G. Gomes, A. C. R. d. Silva, V. S. Candido, R. H. M. Reis, and S. N. Monteiro, "Guaruman: A natural Amazonian fiber with potential for Polymer composite reinforcement," *Materials Research,* vol. 22, (2019).

[12]   C. Oikonomou, *Surface characterization of soft magnetic composite powder*

and compacts: Chalmers Tekniska Hogskola (Sweden), (2014).

[13]   D. S. Mathew and R.-S. Juang, "An overview of the structure and magnetism of spinel ferrite nanoparticles and their synthesis in microemulsions," *Chemical engineering journal,* vol. 129, pp. 51-65, (2007).

[14]   P. V. Shinde, N. M. Shinde, R. S. Mane, and K. H. Kim, "Ferrites for Electrochemical Supercapacitors," in *Spinel Ferrite Nanostructures for Energy Storage Devices*, ed: Elsevier, (2020), pp. 83-122.

[15]   T. N. Pham, T. Q. Huy, and A.-T. Le, "Spinel ferrite (AFe 2 O 4)-based heterostructured designs for lithium-ion battery, environmental monitoring, and biomedical applications," *RSC advances,* vol. 10, pp. 31622-31661, (2020).

[16]   M. USMAN, "Studies of Ferroelectric and Multiferroic Behavior in [Ba (Zr, Ti) O3] 1-y:[CoFe2O4] y System," Quaid-i-Azam University, Islamabad, (2015).

[17]   F. Morin, "Oxides which show a metal-to-insulator transition at the Neel temperature," *Physical review letters,* vol. 3, p. 34, (1959).

[18]   H. Wu, G. Liu, X. Wang, J. Zhang, Y. Chen, J. Shi*, et al.*, "Solvothermal synthesis of cobalt ferrite nanoparticles loaded on multiwalled carbon nanotubes for magnetic resonance imaging and drug delivery," *Acta biomaterialia,* vol. 7, pp. 3496-3504, (2011).

[19]   M. J. Iqbal and S. Farooq, "Enhancement of electrical resistivity of Sr0. 5Ba0. 5Fe12O19 nanomaterials by doping with lanthanum and nickel," *Materials Chemistry and Physics,* vol. 118, pp. 308-313, (2009).

[20]   N. Singh and A. Agarwal, "Preparation, characterization, properties and applications of nano zinc ferrite," *Materials Today: Proceedings,* vol. 5, pp. 9148-9155, (2018).

[21]   G. Thirupathi and R. Singh, "Magnetic properties of zinc ferrite nanoparticles," *IEEE transactions on magnetics,* vol. 48, pp. 3630-3633, (2012).

[22]   B. D. Lee, "Development of material balance evaluation technique (2)," (2000).

[23]   W. Kleemann, "Random-field induced antiferromagnetic, ferroelectric and structural domain states," *International Journal of Modern Physics B,* vol. 7, pp. 2469-2507, (1993).

[24]   K. C. Kao, *Dielectric phenomena in solids*: Elsevier, (2004).

[25] S. Sathiya, K. Parasuraman, M. Anbarasu, and K. Balamurugan, "FT-IR, XRD, and SEM study of CoFe2 O4 nanoparticles by chemical co-precipitation method," *Nano Vision,* vol. 5, pp. 133-138, (2015).

[26] I. Gul and E. Pervaiz, "Comparative study of NiFe2− xAlxO4 ferrite nanoparticles synthesized by chemical co-precipitation and sol–gel combustion techniques," *Materials Research Bulletin,* vol. 47, pp. 1353-1361, (2012).

[27] L. Sagala, S. Humaidi, K. Tarigan, A. Soehada, and P. Sebayang, "Synthesis and characterization of nanoparticles Zn0. 7Ni0. 15Cu0. 15Fe2O4 using the co-precipitation method," in *Journal of Physics: Conference Series*, (2021), p. 012012.

[28] S. B. Khan, S. Irfan, and S.-L. Lee, "Influence of Zn+ 2 doping on Ni-based nanoferrites;(Ni1− x ZnxFe2O4)," *Nanomaterials,* vol. 9, p. 1024, (2019).

[29] S. Sutradhar, S. Das, and P. Chakrabarti, "Magnetic and enhanced microwave absorption properties of nanoparticles of Li0. 32Zn0. 26Cu0. 1Fe2. 32O4 encapsulated in carbon nanotubes," *Materials Letters,* vol. 95, pp. 145-148, (2013).

[30] S. Mahalakshmi and K. S. Manja, "Ac electrical conductivity and dielectric behavior of nanophase nickel ferrites," *Journal of Alloys and Compounds,* vol. 457, pp. 522-525, (2008).

[31] R. Ahmad, I. H. Gul, M. Zarrar, H. Anwar, M. B. Khan Niazi, and A. Khan, "Improved electrical properties of cadmium substituted cobalt ferrites nano-particles for microwave application," *Journal of magnetism and magnetic materials,* vol. 405, pp. 28-35, (2016).

[32] A. Paladino, J. Waugh, J. Green, and A. Booth, "Fine-Grain Nickel Ferrite for Microwave Applications at High Peak-Power Levels," *Journal of Applied Physics,* vol. 37, pp. 3371-3377, (1966).

[33] T. Shanmugavel, S. G. Raj, G. R. Kumar, G. Rajarajan, and D. Saravanan, "Cost effective preparation and characterization of nanocrystalline nickel ferrites (NiFe2O4) in low temperature regime," *Journal of King Saud University-Science,* vol. 27, pp. 176-181, (2015).

[34] M. Arya, M. N. Gandhi, S. S. Prabhu, V. G. Achanta, and S. P. Duttagupta, "Nickel-cobalt-zinc ferrite nanoparticles for radio-frequency/terahertz frequency-selective surface application," *IET Nanodielectrics,* vol. 4, pp. 98-106, (2021).

[35]   R. Kumar, R. R. Singh, and P. Barman, "Cobalt doped nickel zinc ferrite nanoparticles–XRD analyses an insight," *Int J Sci & Eng Res,* vol. 5, pp. 12-20, (2014).

[36]   N. B. Velhal, N. D. Patil, A. R. Shelke, N. G. Deshpande, and V. R. Puri, "Structural, dielectric and magnetic properties of nickel substituted cobalt ferrite nanoparticles: effect of nickel concentration," *AIP Advances,* vol. 5, p. 097166, (2015).

[37]   S. Gibin and P. Sivagurunathan, "Synthesis and characterization of nickel cobalt ferrite (Ni1− xCoxFe2O4) nano particles by co-precipitation method with citrate as chelating agent," *Journal of Materials Science: Materials in Electronics,* vol. 28, pp. 1985-1996, (2017).

[38]   M. Kurian and D. S. Nair, "Effect of preparation conditions on nickel zinc ferrite nanoparticles: a comparison between sol–gel auto combustion and co-precipitation methods," *Journal of Saudi Chemical Society,* vol. 20, pp. S517-S522, (2016).

[39]   C. Ederer and N. A. Spaldin, "Weak ferromagnetism and magnetoelectric coupling in bismuth ferrite," *Physical Review B,* vol. 71, p. 060401, (2005).

[40]   T. Edvinsson, "Optical quantum confinement and photocatalytic properties in two-, one-and zero-dimensional nanostructures," *Royal society open science,* vol. 5, p. 180387, (2018).

[41]   X. Feng, A. Chen, Y. Zhang, J. Wang, L. Shao, and L. Wei, "Application of dental nanomaterials: potential toxicity to the central nervous system," *International journal of nanomedicine,* vol. 10, p. 3547, (2015).

[42]   R. Nagarajan and T. A. Hatton, *Nanoparticles: synthesis, stabilization, passivation, and functionalization*: ACS Publications, (2008).

[43]   F. Ahmad, N. Ashraf, T. Ashraf, R.-B. Zhou, and D.-C. Yin, "Biological synthesis of metallic nanoparticles (MNPs) by plants and microbes: their cellular uptake, biocompatibility, and biomedical applications," *Applied microbiology and biotechnology,* vol. 103, pp. 2913-2935, (2019).

[44]   P. Patnaik, *Dean's analytical chemistry handbook*: McGraw-Hill Education, (2004).

[45]   K. Terada, "Trace elements by coprecipitation: extraction," (2000).

[46]   A. H. Lu, E. e. L. Salabas, and F. Schüth, "Magnetic nanoparticles: synthesis, protection, functionalization, and application," *Angewandte Chemie*

International Edition, vol. 46, pp. 1222-1244, (2007).

[47]   R. Paranthaman, J. Moses, and C. Anandharamakrishnan, "Powder X-ray diffraction conditions for screening curcumin in turmeric powder," *Journal of Food Measurement and Characterization,* pp. 1-9, (2021).

[48]   M. Termtanun, "Photocatalytic degradation of pesticides using TiO2 nanoparticles," University of Nottingham, (2013).

[49]   J. Jalvandi, "Novel chemical and physical approaches for sustainable drug release from biodegradable electrospun nanofibres," RMIT University, (2016).

[50]   D. Stokes, *Principles and practice of variable pressure/environmental scanning electron microscopy (VP-ESEM)*: John Wiley & Sons, (2008).

[51]   D. McMullan, "Scanning electron microscopy 1928–1965," *Scanning,* vol. 17, pp. 175-185, (1995).

[52]   J. I. Goldstein, D. E. Newbury, P. Echlin, D. C. Joy, C. E. Lyman, E. Lifshin*, et al.*, "Special topics in electron beam x-ray microanalysis," *Scanning Electron Microscopy and X-ray Microanalysis: Third Edition,* pp. 453-536, (2003).

[53]   M. Dumont, A. Pyzalla, A. Kostka, A. Borbély, N. Klein, K. Remes*, et al.*, "Characterization of sauropod bone structure," *Biology of the sauropod dinosaurs: Understanding the life of giants, (*2011).

[54]   S. Foner, "The vibrating sample magnetometer: Experiences of a volunteer," *Journal of applied physics,* vol. 79, pp. 4740-4745, (1996).

[55]   S. Foner, "Versatile and sensitive vibrating-sample magnetometer," *Review of Scientific Instruments,* vol. 30, pp. 548-557, (1959).

[56]   D. Dube and R. Natarajan, "Determination of dielectric parameters for films at microwave frequencies," *Journal of Applied Physics,* vol. 44, pp. 4927-4929, (1973).

[57]   F. C. Brown, "The physics of solids," *American Journal of Physics,* vol. 35, pp. 979-979, (1967).

[58]   K. B. Modi, P. Y. Raval, S. J. Shah, C. R. Kathad, S. V. Dulera, M. V. Popat*, et al.*, "Raman and Mossbauer spectroscopy and X-ray diffractometry studies on quenched Copper–Ferri–Aluminates," *Inorganic chemistry,* vol. 54, pp. 1543-1555, (2015).

[59]   S. Lakshmi Reddy, "Infrared spectra in oxide nanocomposites/minerals," *Correlated Functional Oxides: Nanocomposites and Heterostructures,* pp.

117-138, (2017).

[60]   F. Luo and C.-H. Yan, "Anti-phase boundaries pinned abnormal positive magnetoresistance in Mg doped nanocrystalline zinc spinel ferrite," *Chemical Physics Letters,* vol. 452, pp. 296-300, (2008).

[61]   J. Machefert, M. Le Calvar, and M. Lenglet, "FTIR study of nickel and copper oxidation: Theoretical approach and experience," *Surface and interface analysis,* vol. 17, pp. 137-142, (1991).

[62]   B. Lefez, S. Jouen, J. Kasperek, and B. Hannoyer, "Ft-ir microscopic base imaging system: Applications for chemical analysis of zn and ni atmospheric corrosion," *Applied Spectroscopy,* vol. 55, pp. 935-938, (2001).

[63]   M. A. Gabal, "Effect of Mg substitution on the magnetic properties of NiCuZn ferrite nanoparticles prepared through a novel method using egg white," *Journal of Magnetism and Magnetic Materials,* vol. 321, pp. 3144-3148, (2009).

[64]   B. Labde, M. C. Sable, and N. Shamkuwar, "Structural and infra-red studies of Ni1+ xPbxFe2− 2xO4 system," *Materials letters,* vol. 57, pp. 1651-1655, (2003).

[65]   S. Patil, V. Mahajan, A. Ghatage, and S. Lotke, "Structure and magnetic properties of Cd and Ti/Si substituted cobalt ferrites," *Materials chemistry and physics,* vol. 57, pp. 86-91, (1998).

[66]   S. Ahmed, M. F. Mahmood, M. Arifuzzaman, and M. B. Hossen, "Enhancement of electrical and magnetic properties of Al3+ substituted CuZn nano ferrites with structural Rietveld refinement," *Results in Physics,* vol. 30, p. 104833, (2021).

[67]   A. Mahmood and A. Maqsood, "Physical properties, magnetic measurements, dielectric relaxation, and complex impedance studies of cobalt-doped zinc ferrite nanoparticles," *Applied Nanoscience,* vol. 11, pp. 2311-2336, (2021).

[68]   I. Gul, F. Amin, A. Abbasi, M. Anis-ur-Rehman, and A. Maqsood, "Effect of Ag2CO3 addition on the morphology and physical properties of Bi-based (2223) high-Tc superconductors," *Physica C: Superconductivity and its applications,* vol. 449, pp. 139-147, (2006).

[69]   M. A. Rafiq, M. Waqar, Q. K. Muhammad, M. Waleed, M. Saleem, and M. S. Anwar, "Conduction mechanism and magnetic behavior of Cu doped barium hexaferrite ceramics," *Journal of Materials Science: Materials in Electronics,*

vol. 29, pp. 5134-5142, (2018).

[70]   G. Sathishkumar, C. Venkataraju, and K. Sivakumar, "Synthesis, structural and dielectric studies of nickel substituted cobalt-zinc ferrite," *Materials Sciences and Applications,* vol. 1, pp. 19-24, (2010).

[71]   M. L. v. Levin and M. A. f. Miller, "Maxwell's" Treatise on Electricity and Magnetism"," *Soviet Physics Uspekhi,* vol. 24, p. 904, (1981).

[72]   S. Shaat, "Advanced Ferrite Technology," ed: LAMBART, (2012).

[73]   H. Dawoud, L. A-Ouda, and S. Shaat, "Investigation of the effect of Zn ions concentration on DC conductivity and Curie temperature of Ni-spinel ferrite," *American Journal of Materials Science and Application,* vol. 4, pp. 11-17, (2016).

[74]   F. Kremer and A. Schönhals, "Broadband dielectric measurement techniques (10–6 Hz to 1012 Hz)," *Broadband dielectric spectroscopy, (*2012).

[75]   R. Gimenes, M. d. Baldissera, M. Da Silva, C. Da Silveira, D. Soares, L. A. Perazolli*, et al.*, "Structural and magnetic characterization of MnxZn1−xFe2O4 (x= 0.2; 0.35; 0.65; 0.8; 1.0) ferrites obtained by the citrate precursor method," *Ceramics international,* vol. 38, pp. 741-746, (2012).

[76]   A. Volkov and A. Prokhorov, "Broadband dielectric spectroscopy of solids," *Radiophysics and Quantum Electronics,* vol. 46, pp. 657-665, (2003).

[77]   M. E. Hajlaoui, R. Dhahri, N. Hnainia, A. Benchaabane, E. Dhahri, and K. Khirouni, "Conductivity and giant permittivity study of Zn 0.5 Ni 0.5 Fe 2 O 4 spinel ferrite as a function of frequency and temperature," *RSC advances,* vol. 9, pp. 32395-32402, (2019).

[78]   D. E. Gavrila, "Dielectric Spectroscopy, a Modern Method for Microstructural Characterization of Materials," *Journal of Materials Science and Engineering A,* vol. 4, pp. 18-26, (2014).

[79]   J. Li, X. Wang, K. Song, Q. Li, R. Gong, Z. Su*, et al.*, "High magnetic loss Mg–Cu ferrites for ultrahigh frequency EMI suppression applications," *IEEE Transactions on Magnetics,* vol. 51, pp. 1-4, (2015).

[80]   R. Pandit, K. Sharma, P. Kaur, R. Kotnala, J. Shah, and R. Kumar, "Effect of Al3+ substitution on structural, cation distribution, electrical and magnetic properties of CoFe2O4," *Journal of Physics and Chemistry of solids,* vol. 75, pp. 558-569, (2014).

[81]   M. Kaiser, "Electrical conductivity and complex electric modulus of titanium

doped nickel–zinc ferrites," *Physica B: Condensed Matter,* vol. 407, pp. 606-613, (2012).

[82]   M. Rahman, N. Hasan, M. Hoque, M. Hossen, and M. Arifuzzaman, "Structural, dielectric, and electrical transport properties of Al3+ substituted nanocrystalline Ni-Cu spinel ferrites prepared through the sol–gel route," *Results in Physics,* vol. 38, p. 105610, (2022).

[83]   E. Oumezzine, S. Hcini, F. Rhouma, and M. Oumezzine, "Frequency and temperature dependence of conductance, impedance and electrical modulus studies of Ni0. 6Cu0. 4Fe2O4 spinel ferrite," *Journal of Alloys and Compounds,* vol. 726, pp. 187-194, (2017).

[84]   C. Rayssi, S. E. Kossi, J. Dhahri, and K. Khirouni, "Frequency and temperature-dependence of dielectric permittivity and electric modulus studies of the solid solution Ca 0.85 Er 0.1 Ti 1− x Co 4x/3 O 3 (0≤ x≤ 0.1)," *Rsc Advances,* vol. 8, pp. 17139-17150, (2018).

[85]   D. Vollath, W.-V. V. G. KGaA, and Co, "An introduction to synthesis, properties and application," *Management,* vol. 7, pp. 865-870, (2008).

[86]   T. P. Татарчук, "Structural, Optical, and Magnetic Properties of Zn-Doped CoFe2O4 Nanoparticles," (2017).

[87]   M. D. A. M. A. Mahapatra, A. M. A. Das, and D. D. P. Chakrabarti, "Effect of cation distribution on the magnetic and hyperfine behaviour of nanocrystalline Co doped Ni-Zn ferrite," (2015).